doi : 10.17596/0002516

2021-08-31

Cruise Report of KS-21-12

by R/V Shinsei-maru of JAMSTEC/U. Tokyo

Cruise title:
“Interdisciplinary research program in the Tsushima Warm Current — Part I: 3D visualization of wind-generated fine-scale internal waves associated with oceanic eddies”

Yusuke Kawaguchi

[Atmosphere and Ocean Research Institute, The University of Tokyo]

Menu

1. Overview of Research Activities from KS-21-12

Scientific focuses during the Shinsei-maru cruise of KS-21-12 are placed on the key words of Tsushima Warm Current (TWC), warm-core ring (WCR), internal waves, and interdisciplinary effects (i.e. physics-chemistry-biology) (Figure 1). Observation points and ship track were pre-planned by referencing forecasting oceanic model output by Meteorological Research Institute (https://www.jma.go.jp/jma/menu/menureport.html) (Figure 2). The investigations with points above are implemented from two different standpoints: 1) multiply traverses the meso-structure of WCR and 2) investigates it in the Eulerian ways with a mooring system.

1. Physical oceanographic investigation of oceanic eddies that captures internal waves and micro-scale turbulent energy (see Sections 3.1.-3.5. for more detail)
   We attempted to reveal three-dimensional structure and distribution of internal wave packets and its kinetic energy in the context of larger-scale, meso- and/or submeso-scale features, with a special focus on the linkage between wave packet and geostrophic vorticity. During the series of observations, we could successfully collected a number of vertical profiles of microscale turbulence and basic CTD variables using VMP-250 (Rockland Science, Inc.); oceanic current was recorded underway the ship trajectory with 75kHz ship-mounted ADCP (Ocean Surveyer, RDI). Multiple vertical slices of turbulent variables across mesoscale warm-core eddy were obtained during the cruise. Pronounced level of turbulent kinetic energy (TKE) was found as overlapped with larger-scale current structure determined by the quasi-geostrophic (QG) dynamics that also leads baroclinicity in the middle depth. Vigorously meandering feature of TWC front axis distinctly appears, which splits out the WCR with the northern cold waters.

   The series of physical oceanographic data collection was obtained along the two different arrays of meridional and zonal lines, respectively termed to as L-Line and S-Line. On L-Line, consisting of 3 lines, the VMP observation was regularly done at constant spacing of 10 nm, while on S-Line of 5 lines it is at 5 nm. The grid-like VMP survey could make illustrated the virtual distribution of energy-containing wave packets and TKE dissipation rate in the proximities of TWC front and WCR in the Yamato Basin. Some preliminary analysis displays the intricate figure of various physical parameters regarding the microscale turbulence and meso/submeso-scale straining characteristics. Relationship between relative vorticity by QG current and

TKE distribution will be pursued in the future analyses in further detail.

2. Short-term mooring survey of sinking particles under influence of warm-core eddy (Section 3.6)

   Mooring observation was implemented for the clarification of a linkage between geochemical downward flux of particles and physical features represented by quai-geostrophic current and propagating internal waves, both related to a warm-core ring steadily observed in the Yamato Basin. The mooring instrumentation equipped with a couple of sediment traps at middle and deep sites was deployed during early part of KS-21-12, and then successfully recovered during KS-21-13. The data record is nearly two weeks in length. Physical variables such as oceanic current and temperature/salinity were properly collected by using a Longranger ADCP and SeaBird CTD sensors at high frequency of 1 min in sampling rate. For the two-weeks observation, preliminary results are shortly described. From the digital records, mainly of physical part, horizontal current and TS properties tend to be governed by 1) relatively slow geostrophic dynamics, related to the warm-core ring, and 2) short-term oscillations due to near-inertial waves. Chemical analysis is mostly still in progress and to be reported in near future.

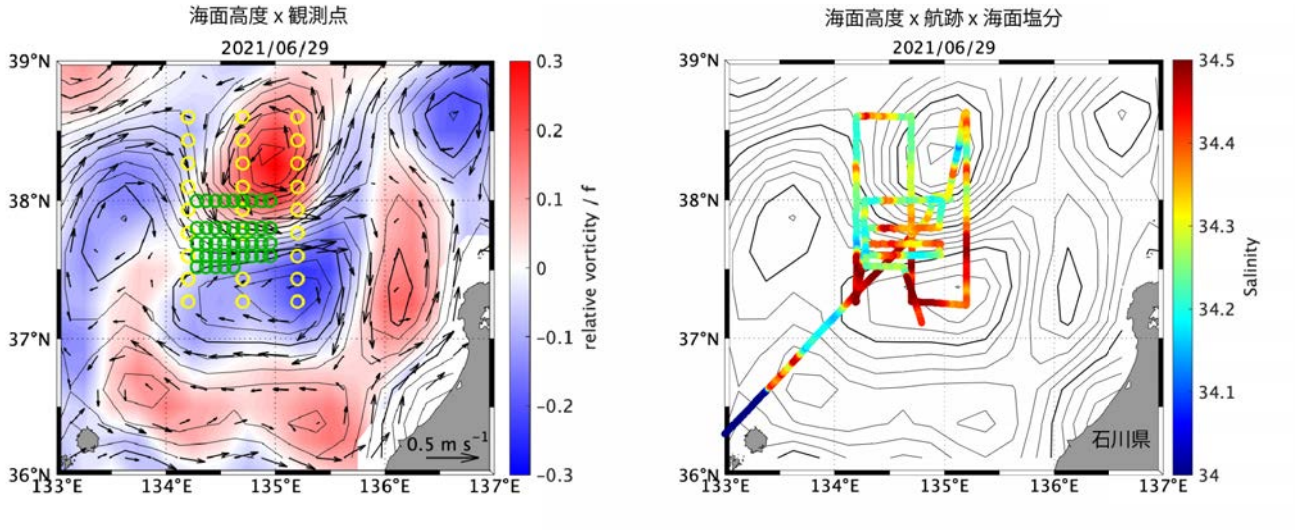

Figure 1: (Left) observational stations (yellow for L-line; green for S-line), with satellite-based absolute dynamic topography (ADT) in color contours and with ADT-based geostrophic current in black vector. (Right) ship track, with surface salinity in color.

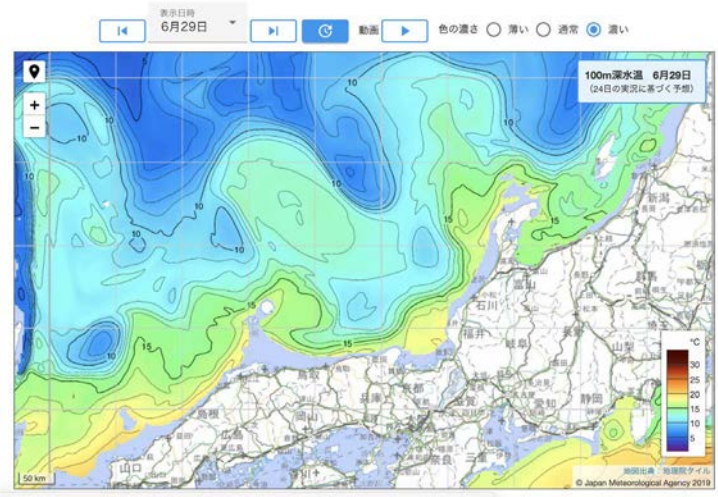

Figure 2: An image of MRI forecasting webpage, depicting predicted temperature field at 100 m depth (for June 29, 2021).

2. Details of KS-21-12 program

(1) Cruise ID: KS-21-12
(2) Name of Vessel: R/V Shinsei-maru of JAMSTEC and The University of Tokyo
(3) Title of cruise:
Interdisciplinary research program in the Tsushima Warm Current — Part I: 3D visualization of wind-generated fine-scale internal waves associated with oceanic eddies
(4) Chief scientist:
Yusuke Kawaguchi
[Atmosphere and Ocean Research Institute, The University of Tokyo]
(5) Cruise period:
from June 25th, 2021 to July 2nd, 2021
(6) Ports:
Departure — Kochi, Kochi Pref.
Arrival — Maizuru, Kyoto Pref.
(7) Research area:
Yamato Basin in the Sea of Japan
(8) List of participants:

Name	Affiliation	Main jobs	Boarding status
Yusuke Kawaguchi, Chief Scientist	AORI, U. Tokyo	All	Onboard
Taku Wagawa	FRA	VMP	Onboard
Shinzou Fujio	AORI, U. Tokyo	Mooring	Onboard
Itsuka Yabe	AORI, U. Tokyo	VMP, CTD, Mooring	Onboard
Daiki Ito	FRA	SADCP	Onboard
Tomoharu Senjyu	RIAM, Kyusyu U.	pCO_2	Onboard
Eun Yae Son	AORI, U. Tokyo	LADCP	Onboard
Akie Sakai	RIAM, Kyusyu U.	XCTD	Onboard
Yu Zeshu	AORI, U. Tokyo	Ocean DNA	Onboard
Sk. Istiaque Ahmed	AORI, U. Tokyo	Ocean DNA	Onboard
Hiroyasu Sato	MWJ	CTD	Onboard
Shigeyoshi Otosaka	AORI, U. Tokyo	Mooring	Not onboard
Shin-ichi Ito	AORI, U. Tokyo	Ocean DNA	Not onboard

Kei Sakamoto	MRI	Modelling	Not onboard

3.1. VMP

(1) Personnel

Yusuke Kawaguchi (PI), Itsuka Yabe (author), EunYae Son, Shinzou Fujio: AORI
Taku Wagawa (author), Daiki Ito: FRA
Tomoharu Senjyu, Akie Sakai: RIAM

(2) Objectives

Direct microstructure measurements with a quasi-free-falling instrument VMP-250 were performed during KS-21-12. This aims to present 3D map of turbulent kinetic energy and diffusivity in the water, which are often explained by some larger scale physical phenomena such as geostrophic balanced motion, internal waves, mesoscale features, and so on.

(3) Instruments and methodology

Regarding the microstructure observations, the VMP-250 (Rockland Science, Inc.) was utilized. The device is loosely tethered from a winch, that is installed on the side deck, and makes it possible the quasi-free falling under only little tension on the line. A couple of fast shear sensors and a single fast temperature sensor (FP07) are installed on the tip of instrument's main body, which collect respectively vertical current shear and vertical temperature gradient at a constant frequency of 512 Hz. The current shear was preliminarily processed by using prepared MATLAB programs (ODAS ver. 4.3) to give 62 vertical profiles of turbulent kinetic energy diffusivity rate, ε, in terms of pressure. The successive profiling of VMP measurements underwent at the sections of Lines L1-L2 and S1–S5 (Figure 1).

(4) VMP deployment positions

Stn.	Cast #	Mon	Day	Start time (JST)		End time (JST)		Latitude		Longitude		File #
				Hour	Min	Hour	Min	Degree	Miin	Degree	Min	
L2-9	1	06	28	10	50	11	04	37	16.0015	134	41.9521	K21-006
L2-8	1	06	28	12	25	12	39	37	26.5083	134	42.0431	K21-007
L2-7	1	06	28	13	51	14	04	37	36.0389	134	42.1003	K21-008
L2-6	1	06	28	15	19	15	36	37	45.9814	134	42.0242	K21-009
L2-5	1	06	28	17	02	17	15	37	56.9695	134	41.9593	K21-011
L2-4	1	06	28	18	40	18	54	38	05.9332	134	41.9185	K21-012
L2-3	1	06	28	20	20	20	34	38	15.9753	134	41.9583	K21-013

L2-2	1	06	28	22	01	22	15	38	25.9726	134	41.9553	K21-014
L2-1	1	06	28	23	42	23	56	38	36.0075	134	41.9212	K21-015
L1-1	1	06	29	02	19	02	33	38	35.9492	134	12.0128	K21-016
L1-2	1	06	29	03	44	03	58	38	25.9465	134	11.9843	K21-017
L1-3	1	06	29	05	07	05	21	38	16.9474	134	11.9507	K21-018
L1-4	1	06	29	06	31	06	45	38	05.9559	134	12.0177	K21-019
L1-5	1	06	29	08	05	08	19	37	55.2619	134	11.8540	K21-021
L1-6	1	06	29	09	25	09	39	37	45.9615	134	12.1791	K21-022
	2	06	29	09	56	10	10	37	45.2302	134	11.9486	Y21-001
L1-7	1	06	29	11	16	11	30	37	35.9362	134	11.9882	Y21-002
L1-8	1	06	29	12	41	12	55	37	26.0784	134	12.0122	Y21-002
L1-9	1	06	29	14	05	14	19	37	14.9948	134	11.9635	Y21-002
S3-9	1	06	29	17	10	17	24	37	41.1761	134	17.0243	Y21-002
	2	06	29	17	56	18	10	37	41.0600	134	17.0258	Y21-002
	3	06	29	18	36	18	50	37	41.1516	134	17.0218	Y21-002
S3-8	1	06	29	19	39	19	53	37	41.1435	134	22.1424	Y21-003
S3-7	1	06	29	20	41	20	55	37	41.1793	134	26.9840	Y21-004
S3-6	1	06	29	21	49	22	03	37	41.0639	134	32.1660	Y21-005
S3-5	1	06	29	22	45	22	59	37	41.1783	134	37.0517	Y21-007
S3-4	1	06	29	23	42	23	56	37	41.1551	134	42.0400	Y21-008
S3-3	1	06	30	00	33	00	46	37	41.2173	134	47.0564	Y21-009
S3-2	1	06	30	01	24	01	38	37	41.1689	134	52.1050	Y21-010
S3-1	1	06	30	02	17	02	30	37	41.2291	134	58.1196	Y21-012
S2-1	1	06	30	03	29	03	42	37	36.1884	134	57.3759	Y21-013
S2-2	1	06	30	04	49	05	02	37	36.1926	134	52.1194	Y21-014
S2-3	1	06	30	06	00	06	13	37	36.1903	134	47.1228	Y21-015
S2-4	1	06	30	07	23	07	36	37	36.1021	134	42.4407	Y21-017
S2-5	1	06	30	08	35	08	48	37	36.1823	134	37.9652	Y21-019
S2-6	1	06	30	09	45	09	58	37	36.1658	134	32.0530	Y21-020
S2-7	1	06	30	10	52	11	05	37	36.0977	134	27.0555	Y21-021
S2-8	1	06	30	11	53	12	06	37	36.2057	134	21.9831	Y21-022
S2-9	1	06	30	12	52	13	05	37	36.1708	134	16.9831	Y21-024
S4-9	1	06	30	14	34	14	47	37	48.0059	134	17.0167	Y21-025
S4-8	1	06	30	15	32	15	45	37	47.9573	134	22.0706	Y21-026
S4-7	1	06	30	16	44	16	57	37	47.9287	134	26.9652	Y21-027

S4-6	1	06	30	17	44	17	57	37	47.9460	134	32.0977	Y21-028
S4-5	1	06	30	18	46	18	59	37	47.9276	134	37.0925	Y21-031
S4-4	1	06	30	19	49	20	02	37	47.9542	134	42.0825	Y21-032
S4-3	1	06	30	20	48	21	01	37	48.0051	134	47.0924	Y21-033
S4-2	1	06	30	21	45	21	58	37	47.9450	134	52.0574	Y21-034
S4-1	1	06	30	22	42	22	55	37	48.0164	134	57.0551	Y21-035
S5-1	1	07	01	00	26	00	39	37	59.9960	134	57.0214	Y21-036
S5-2	1	07	01	01	23	01	36	37	59.9718	134	52.0122	Y21-038
S5-3	1	07	01	02	20	02	33	37	59.9610	134	47.0044	Y21-039
S5-4	1	07	01	03	22	03	35	37	59.9392	134	41.9999	Y21-040
S5-5	1	07	01	04	19	04	32	37	59.9243	134	36.9727	Y21-041
S5-6	1	07	01	05	14	05	28	37	59.9620	134	31.9885	Y21-042
S5-7	1	07	01	06	10	06	23	37	59.9369	134	27.0031	Y21-043
S5-8	1	07	01	07	06	07	19	37	59.9540	134	21.9318	Y21-044
S5-9	1	07	01	08	06	08	19	37	59.9868	134	16.6662	Y21-045
S1-9	1	07	01	11	13	11	26	37	31.2234	134	16.9531	Y21-046
S1-8	1	07	01	12	10	12	23	37	31.2135	134	22.0008	Y21-047
S1-7	1	07	01	13	03	13	16	37	31.1952	134	26.9968	Y21-048
S1-6	1	07	01	13	57	14	10	37	31.2058	134	32.0543	Y21-049
S1-5	1	07	01	14	54	15	07	37	31.2453	134	37.0725	Y21-050

(5) Preliminary Results

Measurements were performed across the mesoscale anticyclonic (centered at 37.4ºN, 135.2ºE and 37.8ºN, 133.6ºE) and cyclonic (38.3ºN, 134.9ºE) eddies. Their water properties respectively corresponded to the Tsushima Warm Current water and the subarctic water. A jet between the eddies (> 0.5 m s^{-1}) is considered to the offshore branch of the Tsushima Warm Current (Figures 1, 3, and 4).

Statistical values for each shear probe were calculated to examine the individual properties. The 5th percentiles (noise level), median, maximum, and interquartile ranges of the energy dissipation rate ε were summarized in Table 1. 19 profiles along Line L were measured by the shear probes, M2254 and M2255, while 43 profiles along Line S were collected by M965 and M960. The range of noise level judged from the 5th percentile was between 1.43×10^{-10} and 7.04×10^{-10} W kg^{-1}(Table 1). The noise levels were slightly higher for M2254 and M2255 than M965 and M960. According to Fig. 2, large values of ε were mainly observed in the surface mixed layer and reached 6.96×10^{-3} W kg^{-1}. The median value of the ε inside of the eddy was 2.6×10^{-9} W kg^{-1}, while that of

underneath the eddy was 9.3×10^{-10} W kg^{-1}.

Overall, the VMP data show the existence of increased dissipation rate, being the magnitude of $\varepsilon = O(10^{-4})$ W kg^{-1}, at the depth of upper 50 m of water column, which is generally coincident with the depth of surface mixed layer (Figures 3 and 4). Those signals are suggestive of the direct mixing due to surface winds or breaking of surface waves. Also, it suggests that the wind-driven turbulent kinetic energy is vertically transported and make it fully energetic over the SML depth.

There was a pycnocline around σ_θ = 26.25–27.00 kg m^{-3}, and high dissipation rates were observed in patches above and below the pycnocline, where *N* was also locally small. This dissipation rate was high under the jet (Figures 3 and 4). Also, it was relatively larger in the anticyclonic eddy than in the cyclonic eddy (Figures 3, 4 and 5).

Eddy diffusivity of density $K_\rho = \Gamma\varepsilon/N^2$ (m^2 s^{-1}) was calculated, where N is the Brunt Väisälä frequency (s^{-1}) and Γ is an efficiency factor. We used the constant value of Γ = 0.2 in this calculation. Figures 6 and 7 show the vertical cross-sections of $\log_{10}(K_\rho)$ along the Line L and Line S. Median values of K_ρ were approximately one order greater than the molecular kinetic viscosity of 1.0×10^{-6} m^2 s^{-1}. (Fig. 8). The values of K_ρ were $O(10^{-6})$ m^2 s^{-1} at the seasonal thermocline located at 20 m (corresponding to 25.0 kg m^{-3}) and the bottom of the eddy structure from 100 m to 300 m (26.0–27.0 kg m^{-3}) (Fig. 6). The median of K_ρ inside of the eddy was 1.3×10^{-5} m^2 s^{-1}.

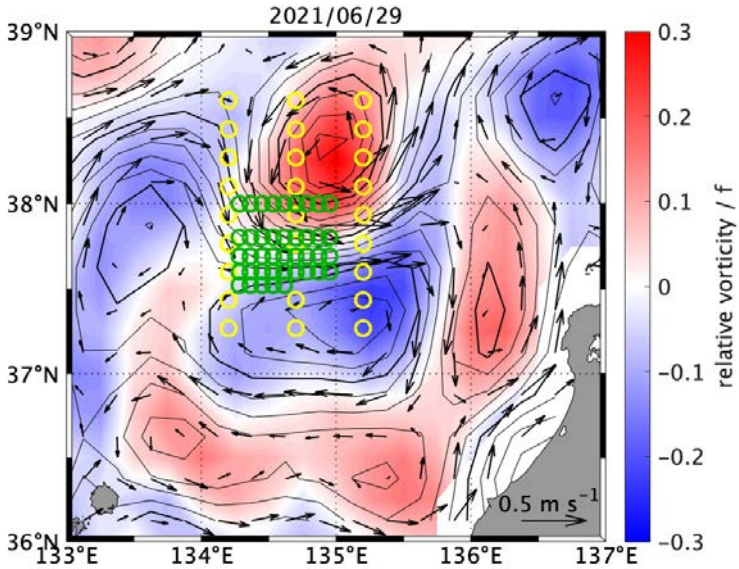

Figure 1. Absolute dynamic topography (m, thin and thick contour intervals 0.02 m and 0.1 m, respectively) and the vertical component of ζ /f (color) on 29 June 2021 when VMP observations were made. Yellow and green open circles respectively represent the measurement points of L-line

Table 1. List of the 5th percentiles, median, maximum, and interquartile range of the energy dissipation rate ε (W kg^{-1}) from each shear probe.

Sensor No.	M2254	M2255	M965	M960
5th percentiles	7.04×10^{-10}	6.89×10^{-10}	1.43×10^{-10}	3.25×10^{-10}
Median	2.26×10^{-9}	2.57×10^{-9}	6.79×10^{-10}	9.75×10^{-9}
Maximum	6.14×10^{-3}	6.96×10^{-3}	1.18×10^{-4}	1.45×10^{-4}
Interquartile range (25–75%)	$1.16e\times10^{-9}$ – 4.42×10^{-9}	1.18×10^{-9} – 6.13×10^{-9}	2.93×10^{-10} – 1.43×10^{-9}	5.29×10^{-10} – 1.94×10^{-9}

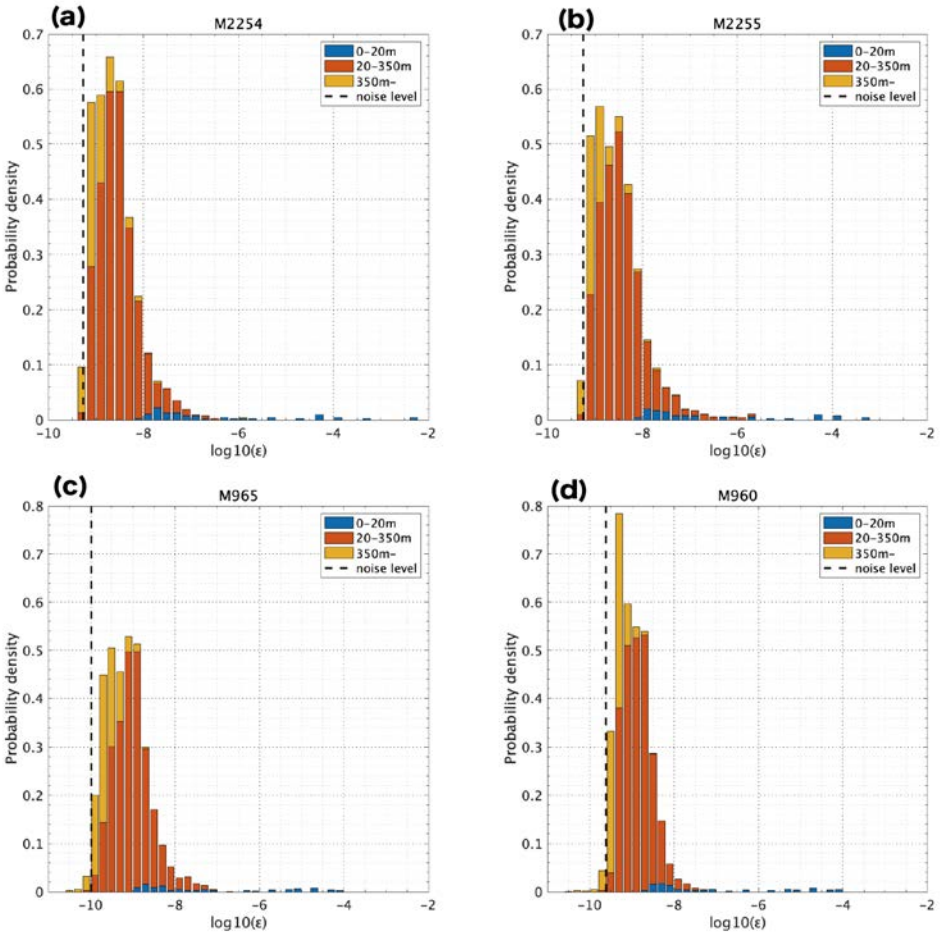

Figure 2. Histogram of the energy dissipation rate $\log_{10}(\varepsilon)$ (W kg^{-1}) for probe numbers of (a) M2254, (b) M2255, (c) M965, and (d) M960. Probability densities were calculated in three layers, i.e., the surface mixed layer (shallower than 20 m, blue), inside of the eddy structure (20–350 m, red), and underneath the eddy (350 m and deeper, yellow). Black dashed lines indicate the noise level of $1.43–7.04\times10^{-10}$ W kg^{-1} (Table 1).

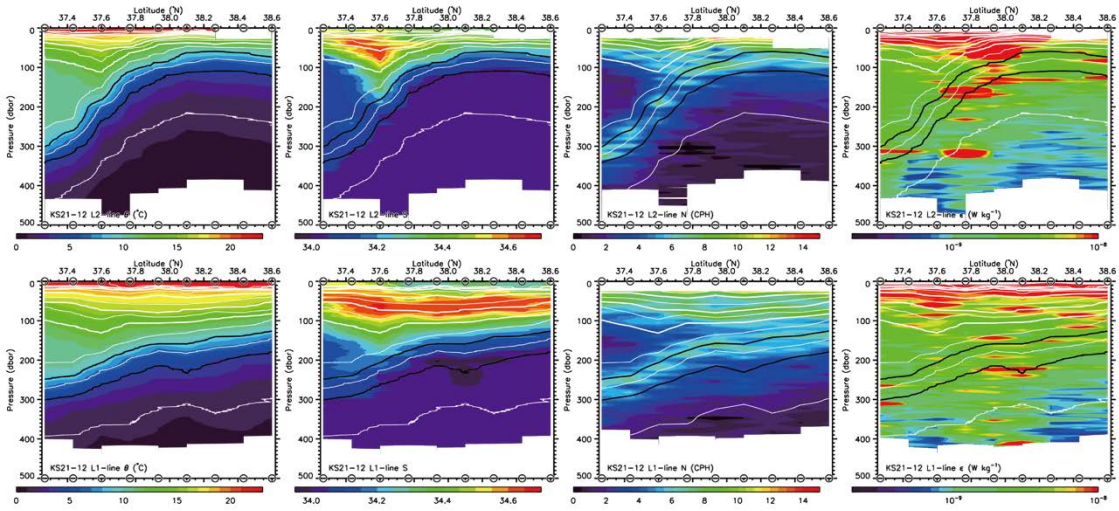

Figure 3. Vertical cross-sections of potential temperature, salinity, buoyancy frequency, and the dissipation rate ϵ along Line L (Line L1 to L2 from bottom to top). ϵ is chosen as the smaller of the value of ε_1 and ε_2 from Shear 1 and Shear 2 sensors. Thin and thick contours respectively show potential density at intervals of σ_θ=0.25 kg m^{-3} and σ_θ=0.5 kg m^{-3}. Thick black contours show the isopycnals corresponding to σ_θ=26.5 and 27.0 kg m^{-3}.

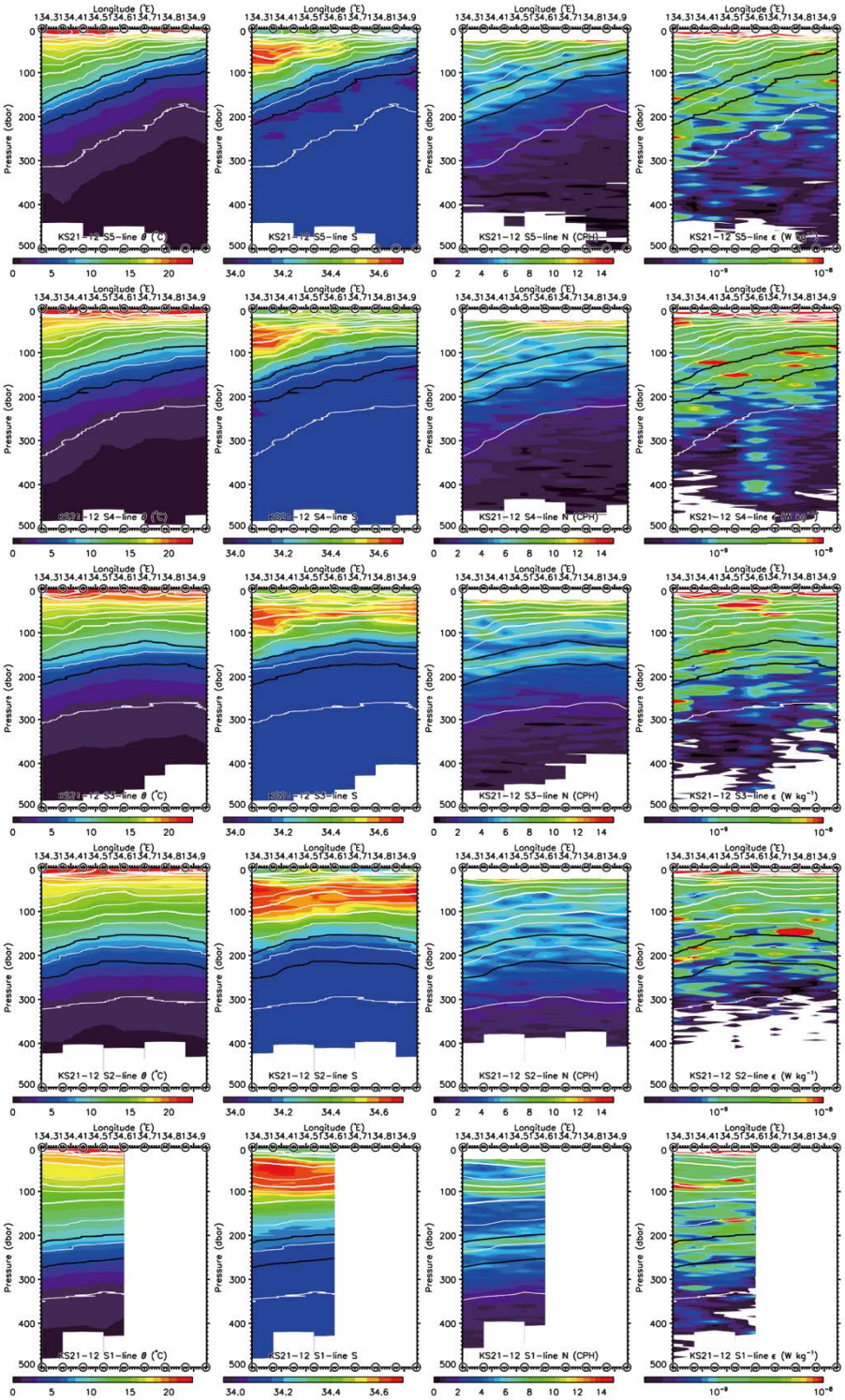

Figure 4. Same as Figure 2, except for Line S.

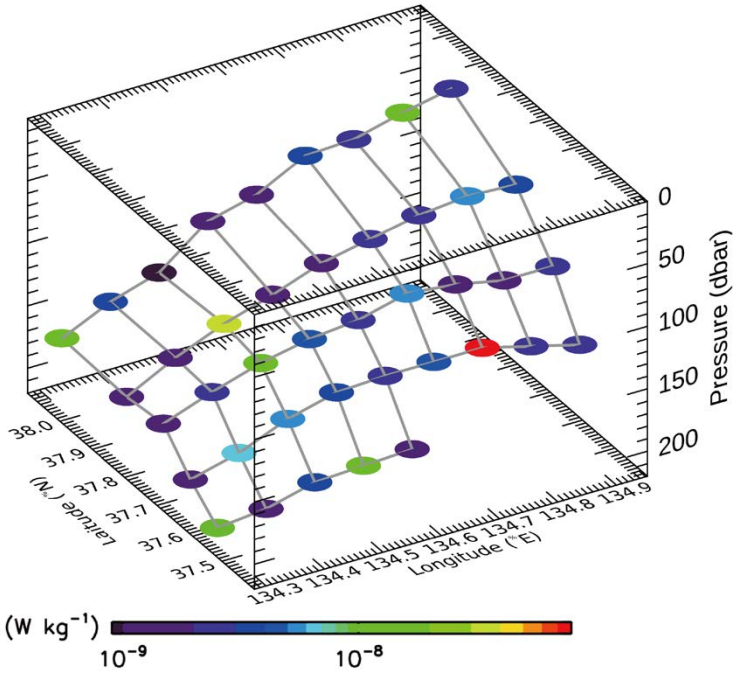

Figure 5. 3D-map of ε (maximum value over σ_θ=26.25–26.5 kg m^{-3}) on the isopycnal of σ_θ=26.4 kg m^{-3}.

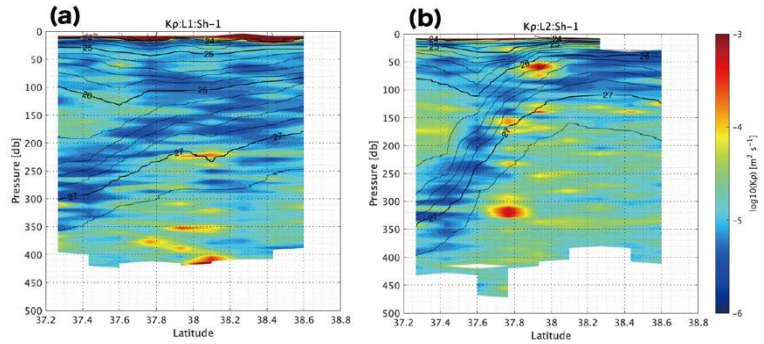

Figure 6. Vertical cross-sections of eddy diffusivity of density $\log_{10}(K_\rho)$ (m^2 s^{-1}) along Line (a) L1 and (b) L2. K_ρ from Shear 1 sensor was selected. Thin and thick contours respectively show potential density at intervals of σ_θ=0.2 kg m^{-3} and σ_θ=1.0 kg m^{-3}.

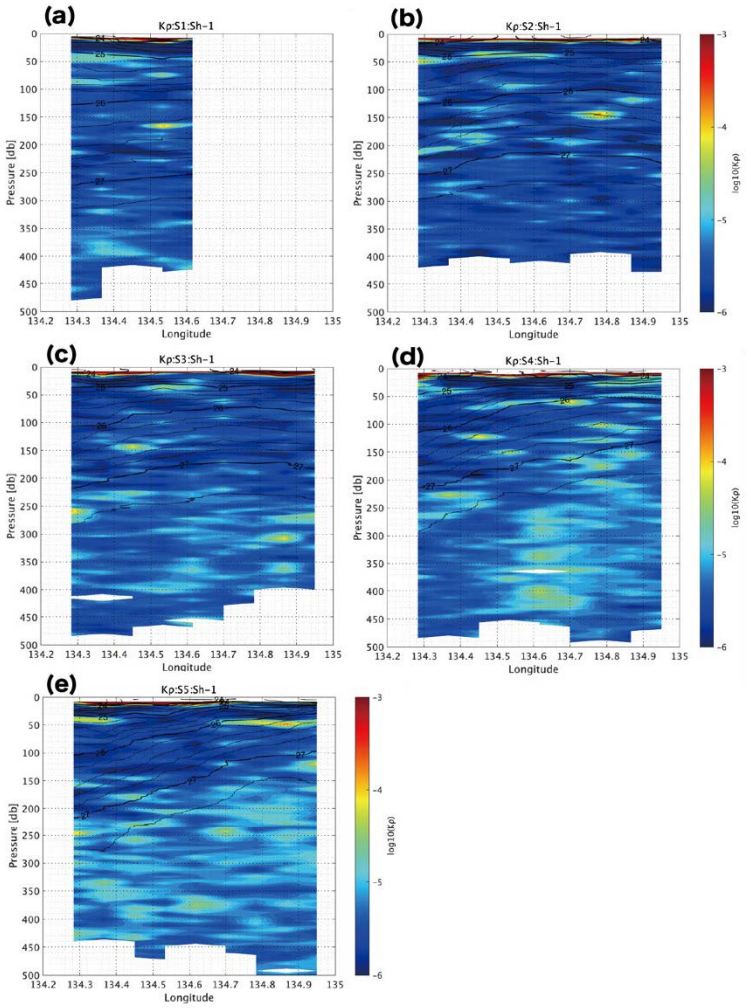

Figure 7. Same as Figure 6, except for Line (a) S1, (b) S2, (c) S3, (d) S4, and (e) S5.

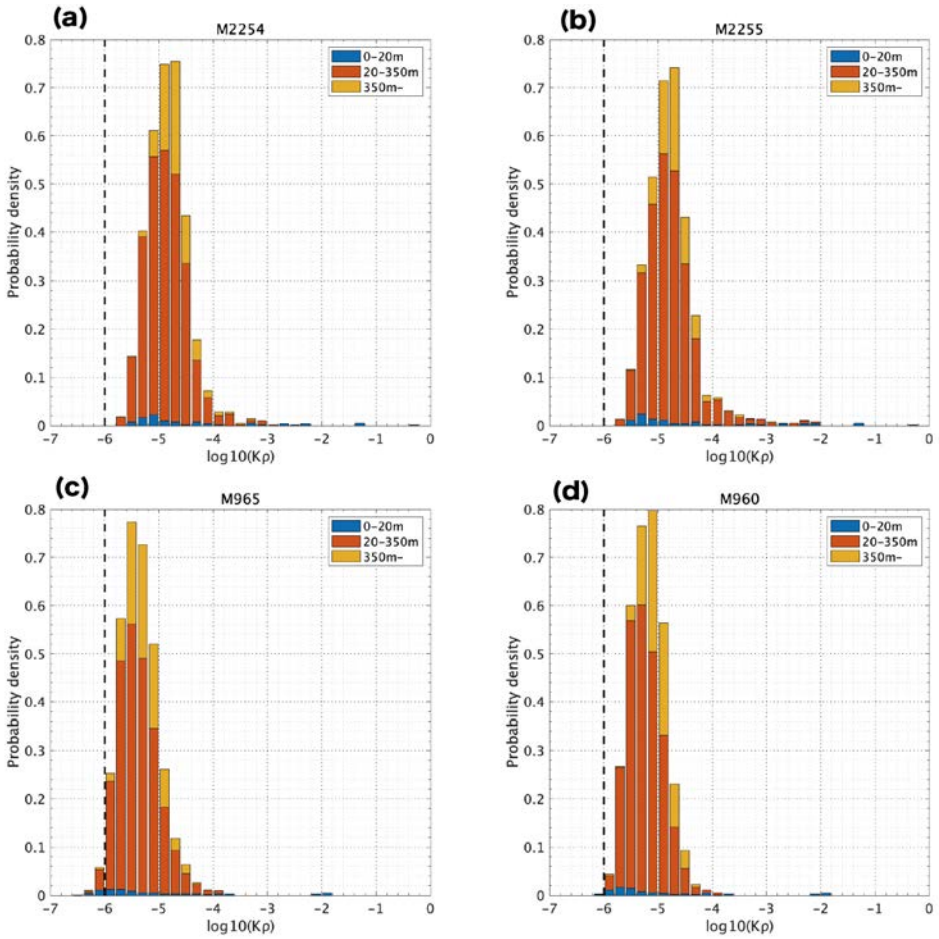

Figure 8. Histogram of the eddy diffusivity of density $\log_{10}(K_\rho)$ (m^2 s^{-1}) for probe numbers of (a) M2254, (b) M2255, (c) M965, (d) M960. Probability densities were calculated in three layers, i.e., the surface mixed layer (shallower than 20 m, blue), inside of the eddy structure (20–350 m, red), and underneath the eddy (350 m and deeper, yellow). Black dashed lines indicate the molecular kinetic viscosity of 1.0×10^{-6} m^2 s^{-1}.

3.2. SADCP

(1) Personnel

Daiki Ito, FRA (author of description)
Yusuke Kawaguchi, AORI, PI

(2) Objectives

Eastward (u) and northward (v) current velocities were continuously observed by a shipboard acoustic Doppler current profiler (SADCP) to examine velocity structures along the ship track.

(6) Instruments and methodology

2-1) Data processing

RDI 38-kHz SADCP was used. The corrected data were averaged into time bins of 5 min by intervals of 16 m in depth. Misalignment angle was estimated from the ship velocities measured by a Global Positioning System (GPS) and by bottom tracking ADCP data, and the data were calibrated for the misalignment angle (0.064). Data with percent good 4 (PG4) larger than 70 were used in the analysis.

2-2) Horizontal shear

The velocities were simply further time-averaged so that mean values between the XCTD/VMP stations are obtained to see the synoptic velocity structure. In addition, to estimate the dominance of strain and eddy motion, horizontal velocity shears were calculated. The x and y derivative (x- and y-axis were defined positive eastward and northward, respectively) of velocities (u_x, v_x, u_y, and v_y; subscripts denote derivatives) was calculated across (along) and along (across) the L-lines (S-lines), respectively.

The strain- and eddy- dominated areas were further visualized by calculating Okubo-Weiss parameter (W) and lateral strain rate (α) using time-averaged velocities derived as:

$$W = \sigma_n^2 + \sigma_s^2 - \omega^2,$$

$$\alpha = \left[\left(u_x - v_y\right)^2 + \left(v_x + u_y\right)^2\right]^{1/2},$$

where $\sigma_n = u_x - v_y$ and $\sigma_s = v_x + u_y$ are the normal and shear components of strain and $\omega = v_x - u_y$ is the relative vorticity. Positive and negative values of W are interpreted as dominance of strain and eddy motion, respectively. Large values of α, typically larger than 1.6×10^{-5} s^{-1}, was a measure of tendencies of frontogenesis and frontolysis driven by large-scale and mesoscale horizontal convergence and divergence.

2-3) Vertical shear

To examine the vertical shear of horizontal velocities, vertical difference of u and v (u_z and v_z, respectively; z-axis was defined positive upward) was also calculated using the data of ±10 m.

(7) Preliminary Results

3-1) Horizontal map

Horizontal velocity at a depth of 200 m along the ship track (Fig. 1) was basically consistent with distribution of mesoscale eddies on the satellite sea surface height (SSH) map produced by AVISO (https://www.aviso.altimetry.fr); that is, counterclockwise flow associated with a cyclonic eddy centered at 134°50'E, 38°20'N and clockwise flow around an anticyclonic eddy centered at 134°40', 37°10'N were obvious. Strong eastward velocity (~ 0.6 m s^{-1}) was in the downstream region between the anticyclonic eddy and the cyclonic eddy. Between these two eddies, convergence (divergence) in the cross-frontal direction were expected in the downstream (upstream) region.

3-2) L-line

3-2-1) General structure

The positive values of u corresponding to the front (centered at 37º40'N) reached to a depth of 300 m along L1 and to 600 m along L3 (Figure 2). As seen in Fig. 1, convergence (divergence) tendency across the front was in the surface layer along L1 and L2 (L3) (v in Figure 2). The time-averaged velocity (Figure 3) showed that noises that seemed to be due to changes of vessel speed were removed, and the synoptic velocity structure is seen clearly.

3-2-2) Horizontal shear

The x derivative of velocities (Figure 4) was small compared with the y derivative (Figure 5), but positive u_x was seen near the front, which mean that u increased in the downstream region. On the south side of the front, v_x was positive in the upstream region (Figure 4a) while negative in the downstream (Figure 4b), also suggesting the divergent flow in the downstream. The strengthen of u along the front with increasing longitude was also seen in the u_y distribution (Figure 5) that increase and decrease steeply south and north of fronts, respectively. On the other hand, v_y was negative along L1 and L2 whereas was positive along L3 near the front, which emphasized the convergence and divergence in the cross-frontal direction in the upstream and downstream region, respectively.

Near the front in particular in the upstream region, W and α showed large positive values (Figure 6a) that suggest the strain at the frontal region and evolving tendency of the front. In the downstream region, on the other hand, the vortex flow was dominant in the south and north of the core of eastward flow (around 37°40'N), although the strain was seen near the core. This velocity structure suggested that the effect of strain due to the approach of the cyclonic and anticyclonic eddies was large in the upstream region, while, in the downstream region, the effect of the rotating flow driven by the anticyclonic (cyclonic) eddy on the south (north) side of the front became dominant (cf. Figure 1).

3-2-3) Vertical shear

Organized pattern of large positive u_z was along the pycnocline in the frontal region (Figure 7). In other areas, vertical scales of patches of u_z and v_z were small compared with horizontal gradient of velocities (Figures 4–6), suggesting that the fine vertical velocity shear affected the mixing in this region.

3-3) S-line

3-3-1) General structure

The values of u were large toward the south and east (Figure 8), and the largest u (larger than 0.8 m s^{-1}) was observed along S2 (Figure 8d), which corresponded to the eastward flow at the front seen in L2 and L3 (Figure 2). The values of v were generally negative in the surface layer along the north lines (Figures 8a and 8b) corresponding to southward flow driven by the cyclonic eddy. The positive values of v appeared in the east of lines with going to the south (Figures 8c and 8d), which in turn related to the northward flow of the cyclonic eddy. Meanwhile, noises in the form of vertical streaks at the VMP stations were removed after time-averaging (Figure 9) same as L-line (Figure 3).

3-3-2) Horizontal shear

The increase of u in the surface layer with increasing longitude and decreasing latitude resulted in the positive value of u_x (Figure 10). In addition, patches of shear flows with smaller scale than those along L-line were found in the subsurface layer, which was likely due to the high horizontal resolution of data. The values of v_x were also positive near the surface, which was consistent with the northward flow captured in the east of lines (Figures 8 and 9). Reflecting the increase of u toward the south in the surface layer, negative values of u_y were broadly seen between S2 and S5 (Figures 11a–c) above 200-m depth, although the values turned positive between S1 and S2 (Figure 11d). In the

subsurface layer below 200-m depth, on the other hand, the positive u_y was found especially between S2 and S3 and in the west side between S3 and S4 (Figures 11b and 11c), suggesting the difference of velocity structure between the upper and lower layer. Because the southward flow was strong with increasing latitude, v_y was also negative above 200-m depth (Figure 11) except for the east side between S1 and S2 where northward current existed (Figure 11d).

The values of W showed complex patterns (Figure 12) especially above the 200-m depth compared with those along L-line (Figure 6). In particular, between S2 and S3 (Figure 12c), large negative and positive values of W were distributed close to each other. Although this pattern likely suggested that the shear flows had small-scale variation near the strong eastward flow in the frontal region, to examine synoptic velocity field, further processing will be required such as vertical and horizontal filtering and estimation of absolute geostrophic velocity using temperature and salinity data.

Although the pattern of W was complex even in the surface layer near the front where strong eastward flow was observed, the values of α was broadly positive near the surface (Figure 12). This distribution was the basis for the evolution of the front near S1–S3 lines. Corresponding to the patches of positive W, the large values of α ($> 2.0 \times 10^{-5}$ s^{-1}) was found in the subsurface layer below the broad positive values. As with the values of W, the validity of the distribution of α needs to be verified by applying filter processing.

3-3-3) Vertical shear

Large positive u_z was recognized especially along S1–S3 (Figure 13) associated with the strengthen of surface eastward toward the south of the observed region. Unlike L-line (Figure 7), the large values were in horizontal streaks, probably due to the fact that survey lines were mostly along the front. Large negative v_z, on the other hand, was centered at the west side of lines S3–S5 (Figures 13a–c) caused by the southward flow in the surface layer. We need to examine the correspondence with hydrographic structure and turbulent mixing process.

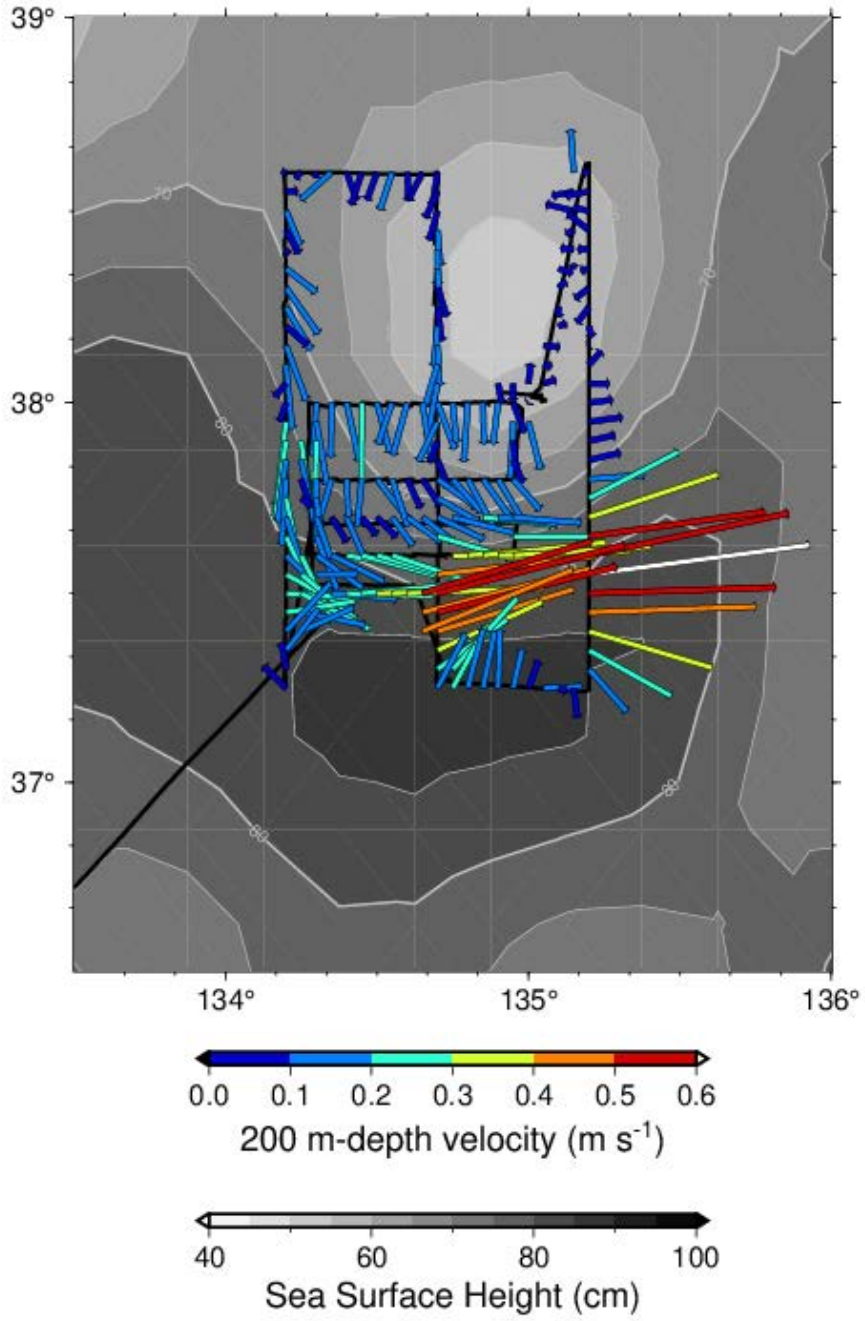

Figure 1. Horizontal velocity along the ship track at a depth of 200 m on sea surface height map on June 27, 2021.

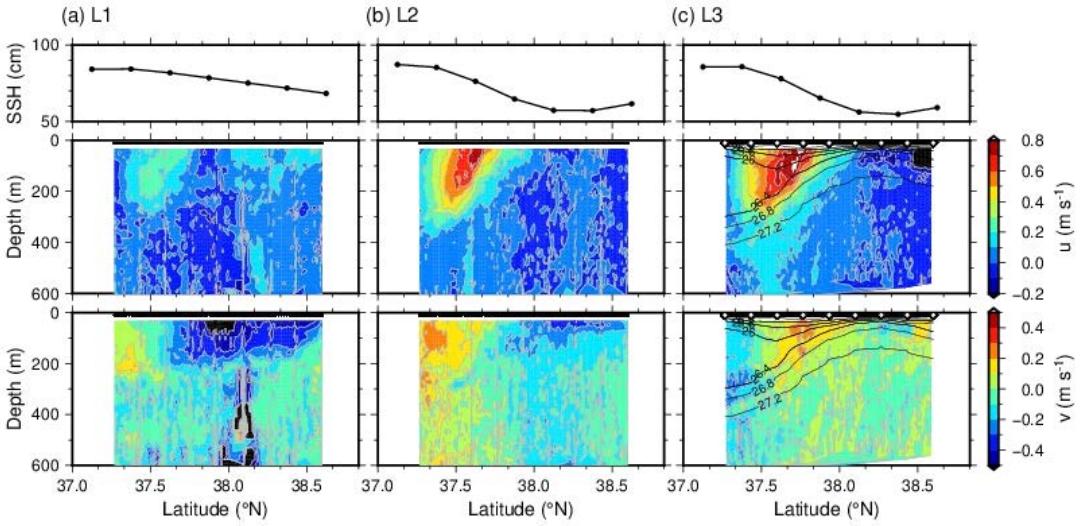

Figure 2. (top) SSH (cm) and sections of (middle) *u* (m s^{-1}) and (bottom) *v* (m s^{-1}) along **a**–**c** L1–L3. Black dots at the top of the sections indicate positions of SADCP data. Black line in **c** denote potential density with a contour interval of 0.4 kg m^{-3} from 25.6–27.2 kg m^{-3}. White diamonds at the top of the section in **c** indicate the XCTD stations.

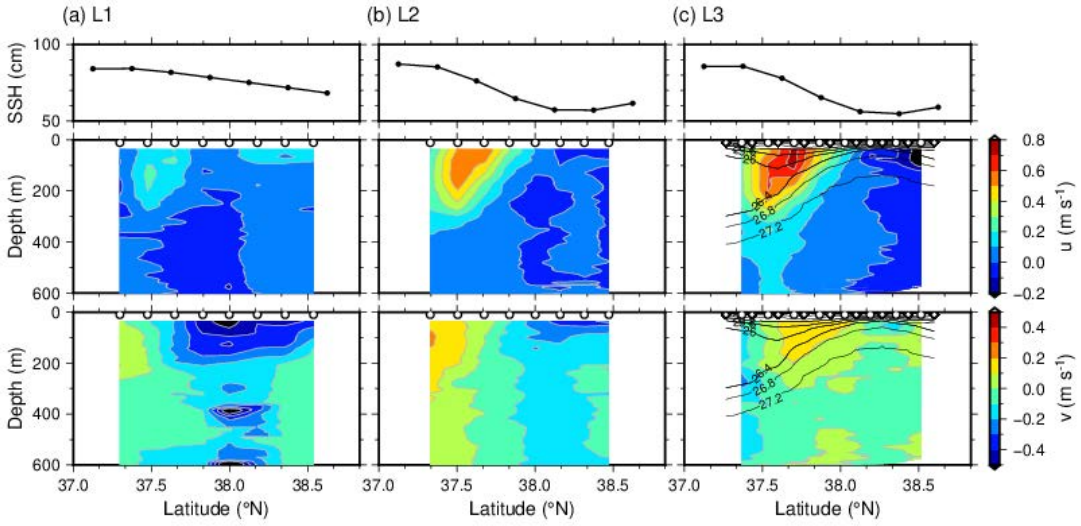

Figure 3. As in Fig. 2, but for time-averaged values to obtain the mean values between XCTD/VMP stations. White circles at the top of sections denote positions of mean values.

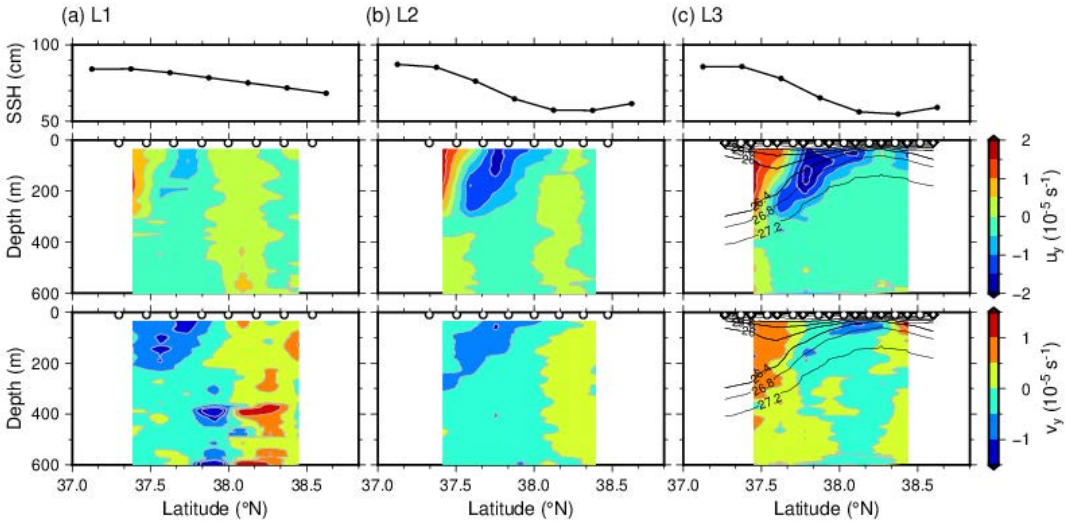

Figure 4. Sections of (middle) u_x and (bottom) v_x between **a** L1 and L2, and **b** L2 and L3. White circles at the top of sections denote positions of mean values of velocities.

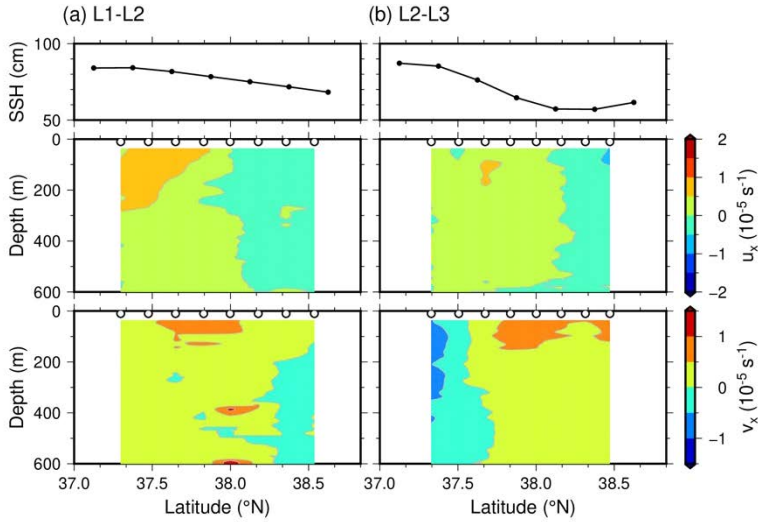

F**igure 5**. Sections of (middle) u_y and (bottom) v_y along **a** L1, **b** L2, and **c** L3. White circles at the top of sections denote positions of mean values of velocities.

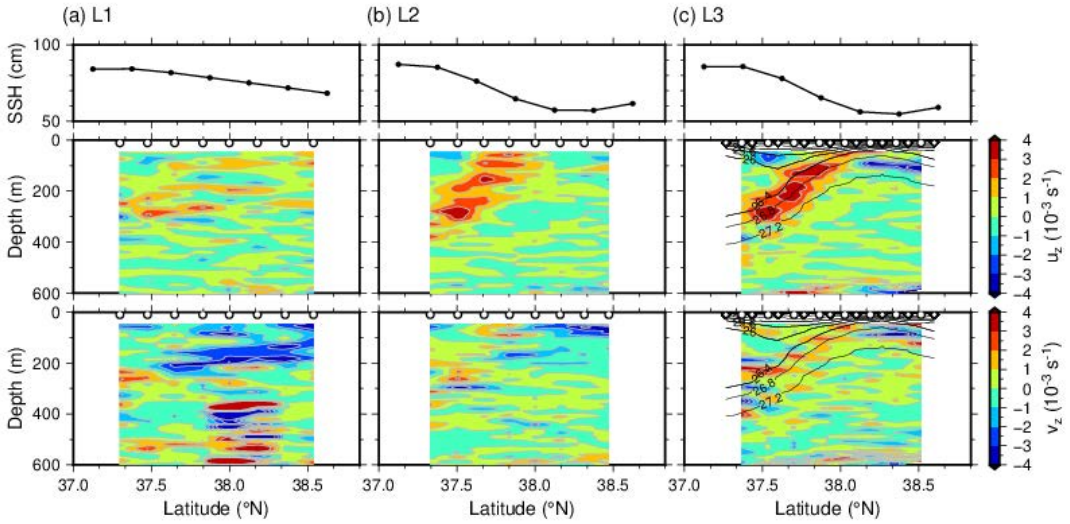

Figure 6. As in Fig. 4, but for (middle) Okubo-Weiss parameter (W) and (bottom) lateral strain rate (α).

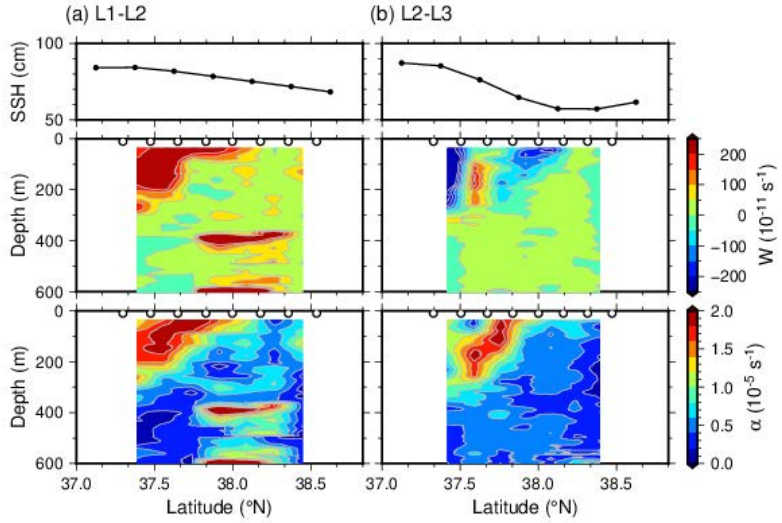

Figure 7. As in Fig. 5, but for (middle) u_z and (bottom) v_z.

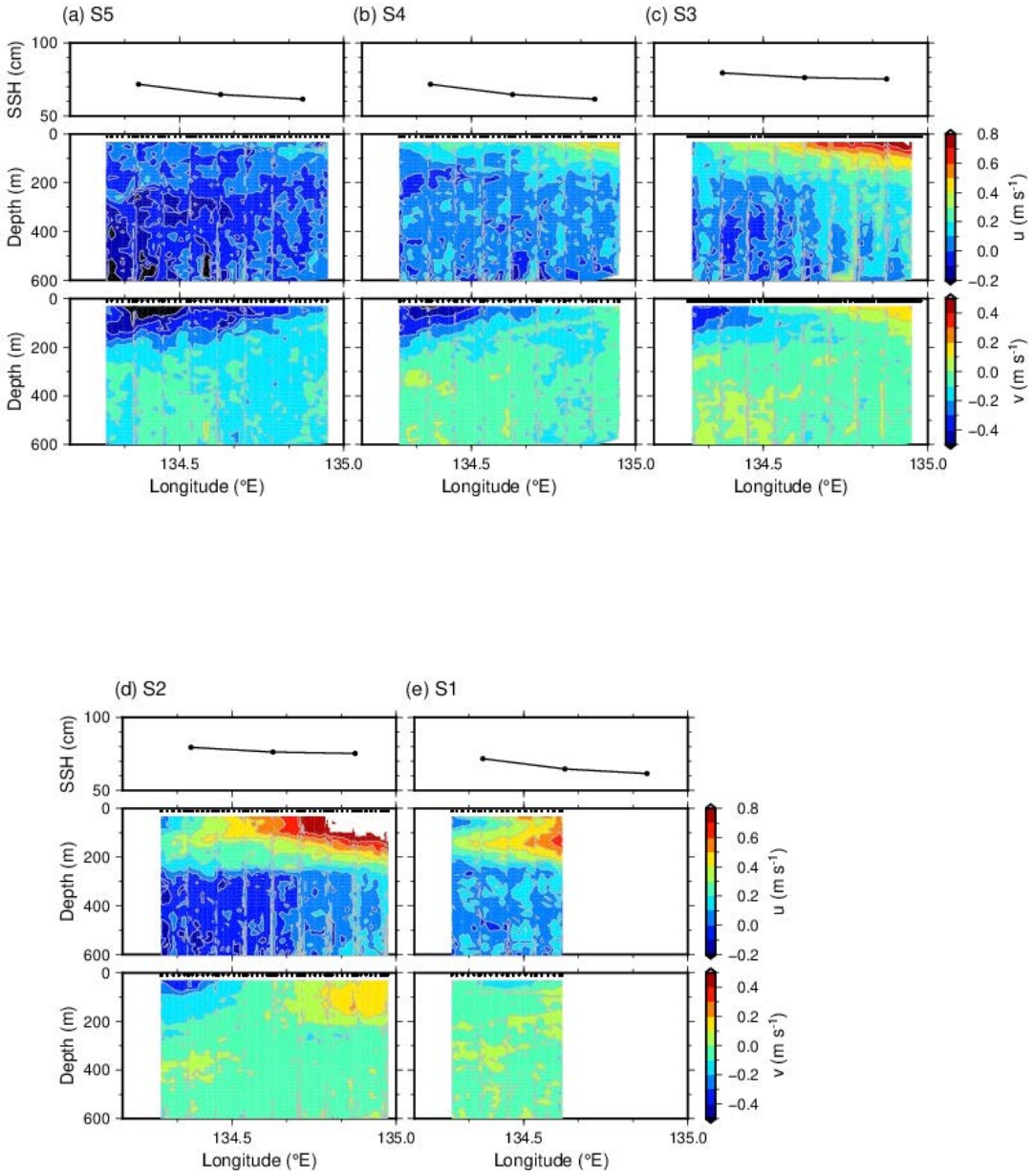

Figure 8. As in Fig. 2, but for **a**–**e** S5–S1.

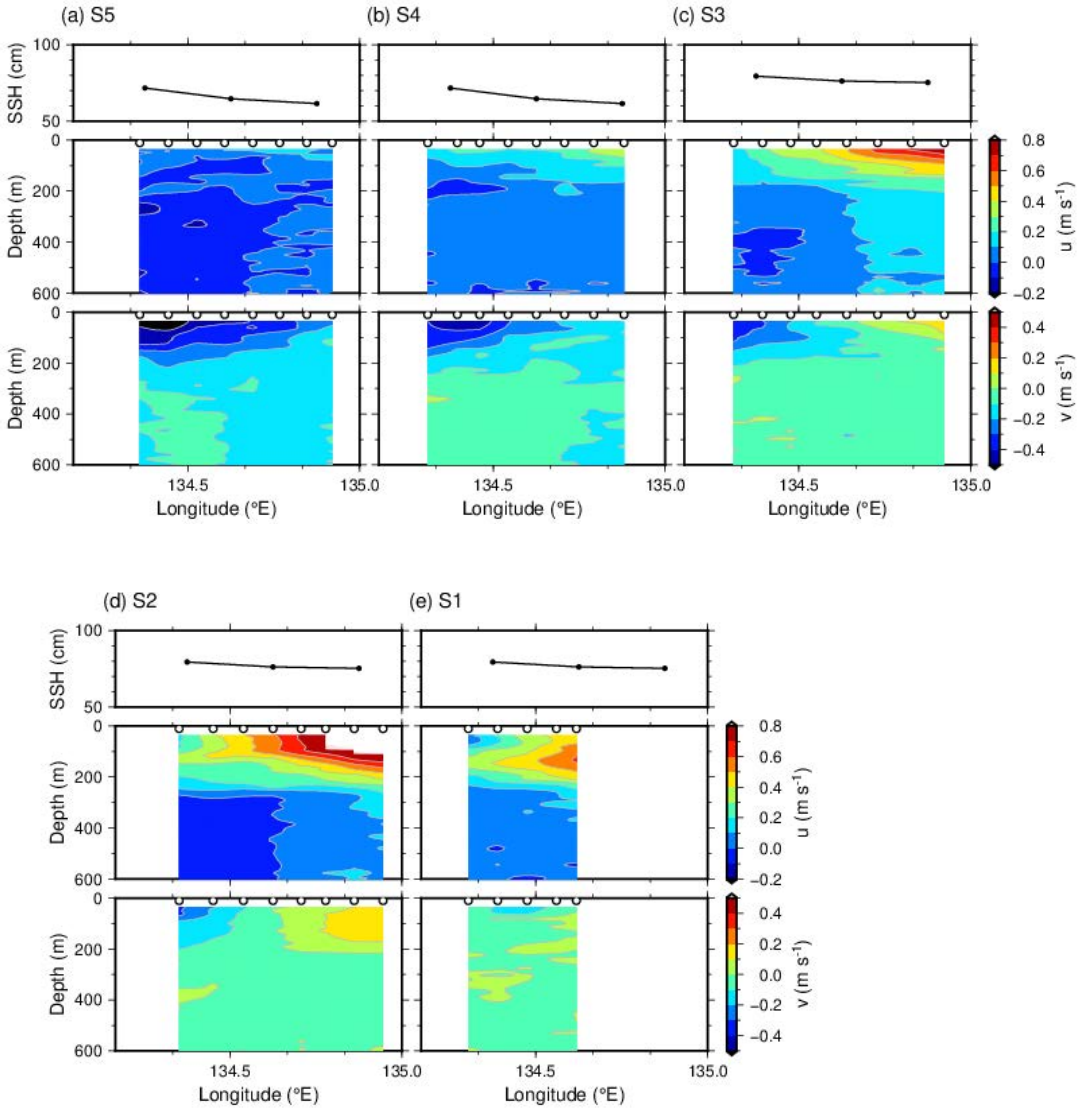

Figure 9. As in Fig. 3, but for **a**–**e** S5–S1.

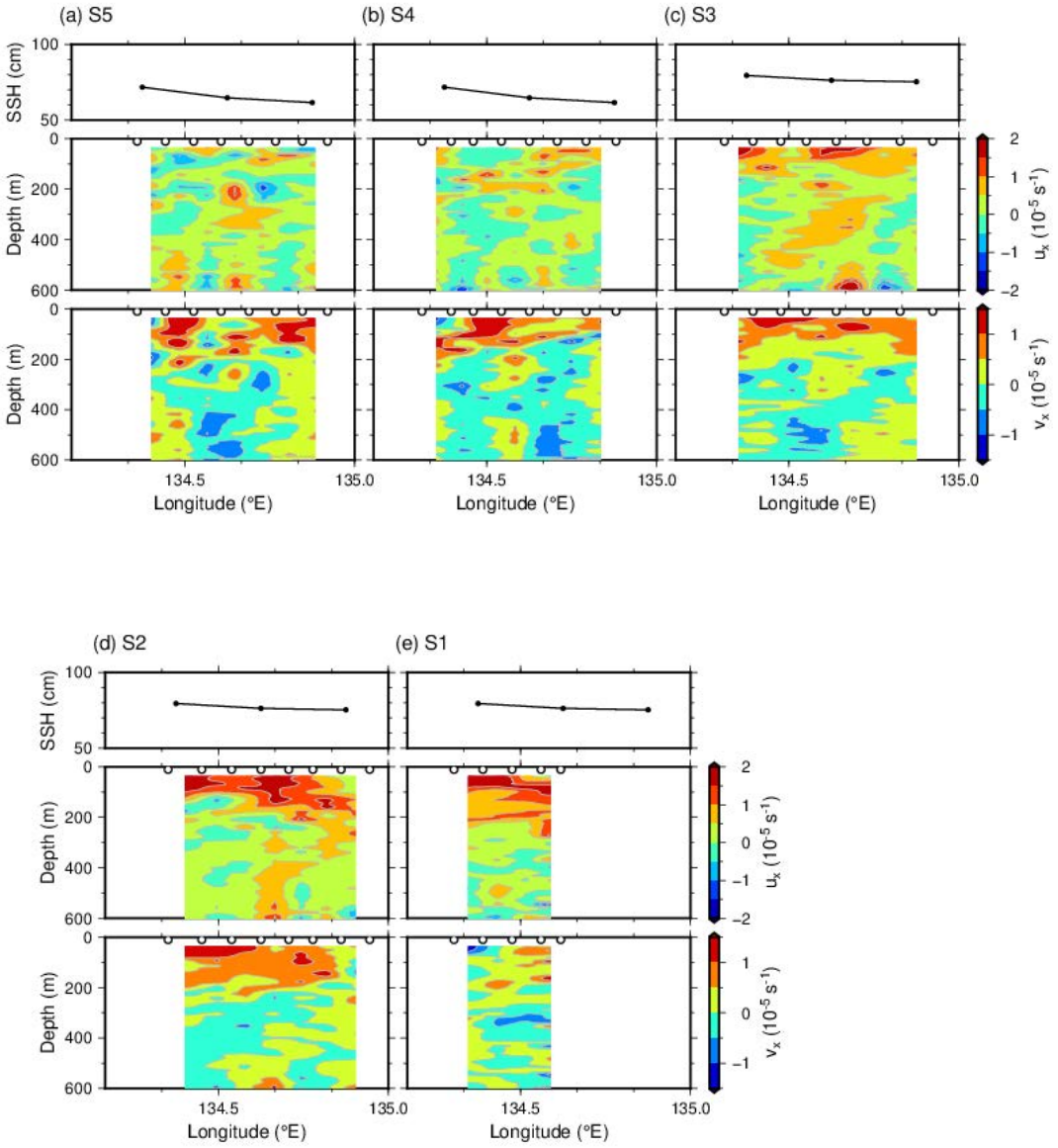

Figure 10. As in Fig. 4, but for **a**–**e** S5–S1.

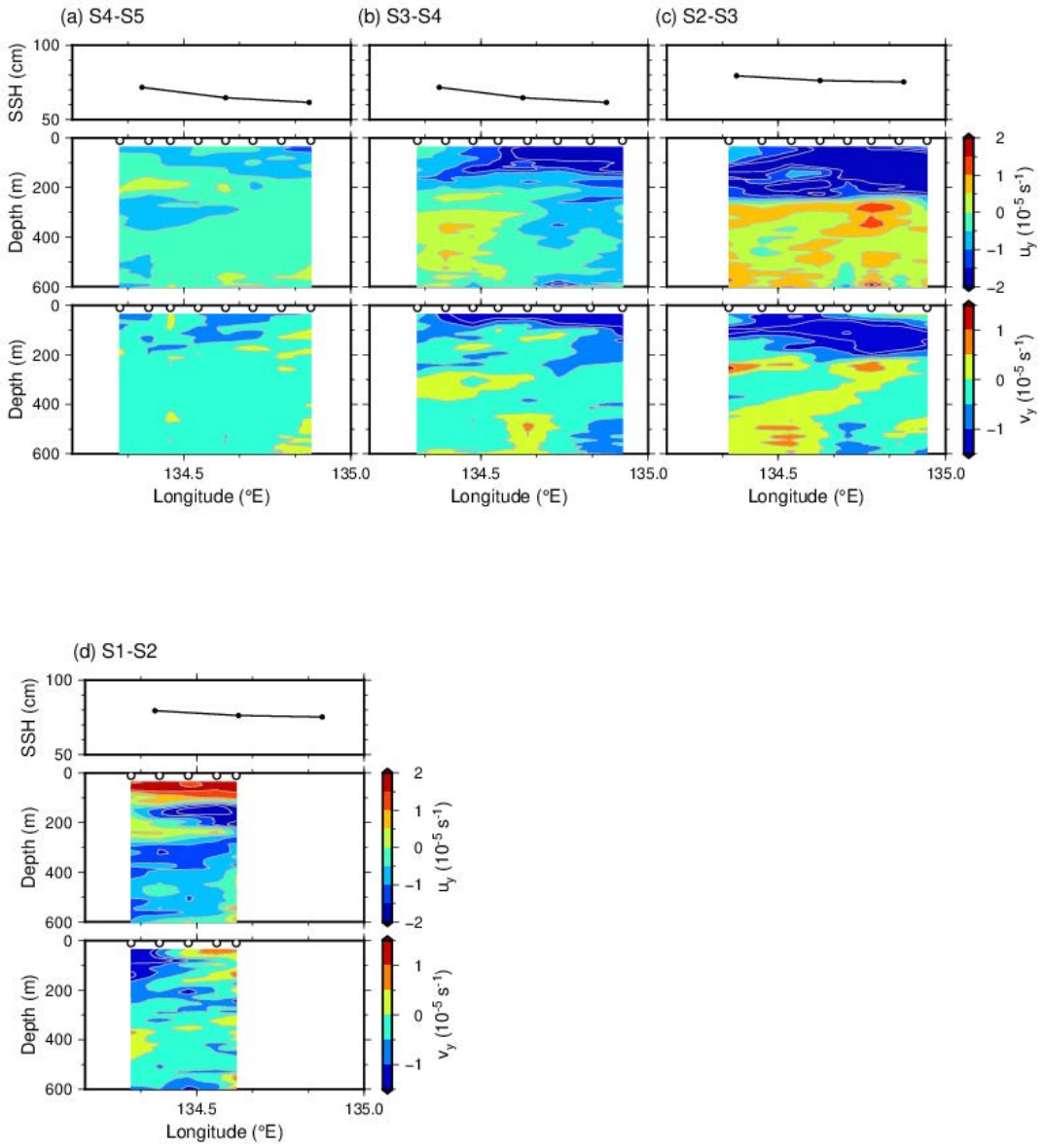

Figure 11. As in Fig. 5, but for between **a** S4 and S5, **b** S3 and S4, **c** S2 and S3, and **d** S1 and S2.

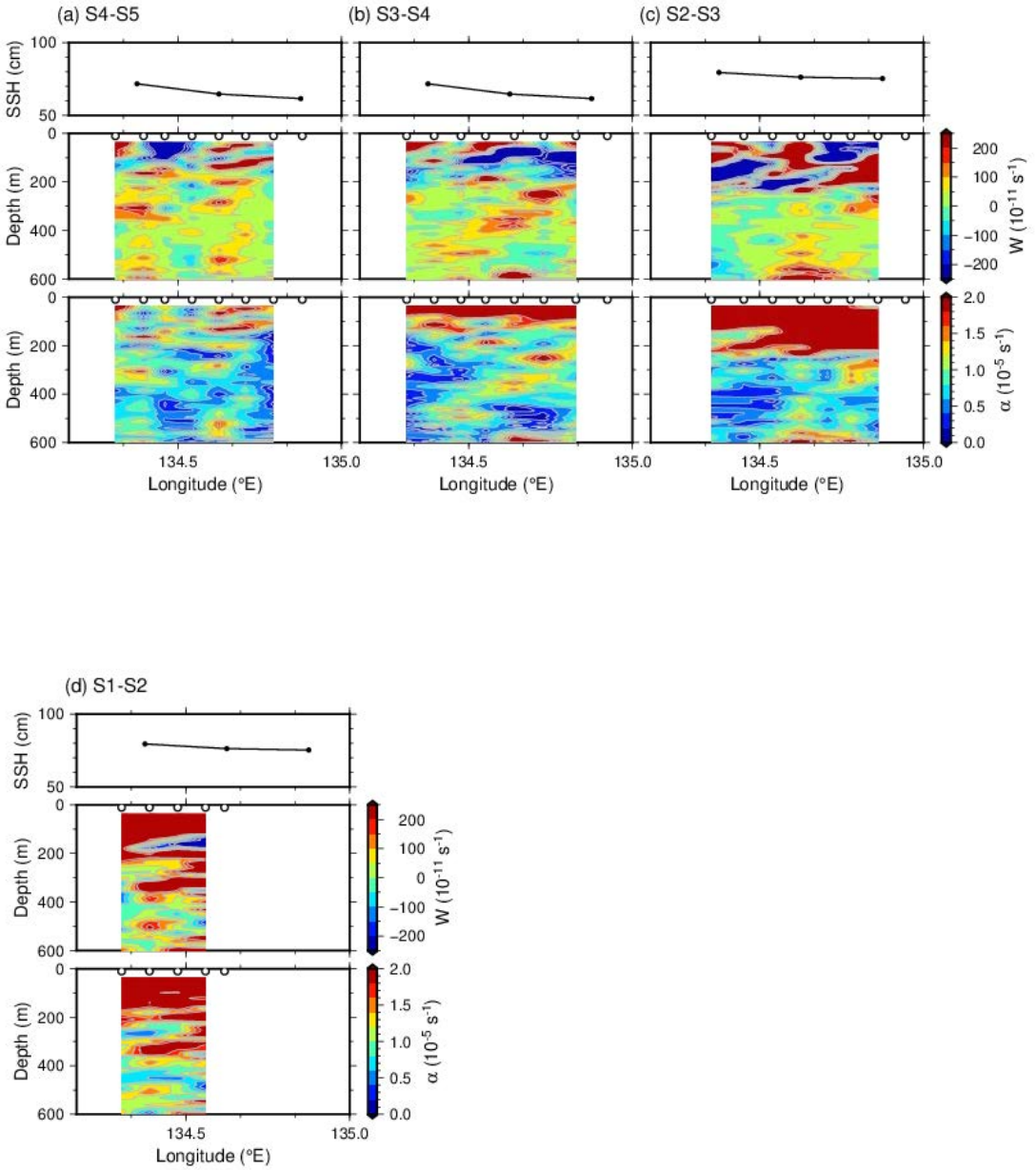

Figure 12. As in Fig. 6, but for between **a** S4 and S5, **b** S3 and S4, **c** S2 and S3, and **d** S1 and S2.

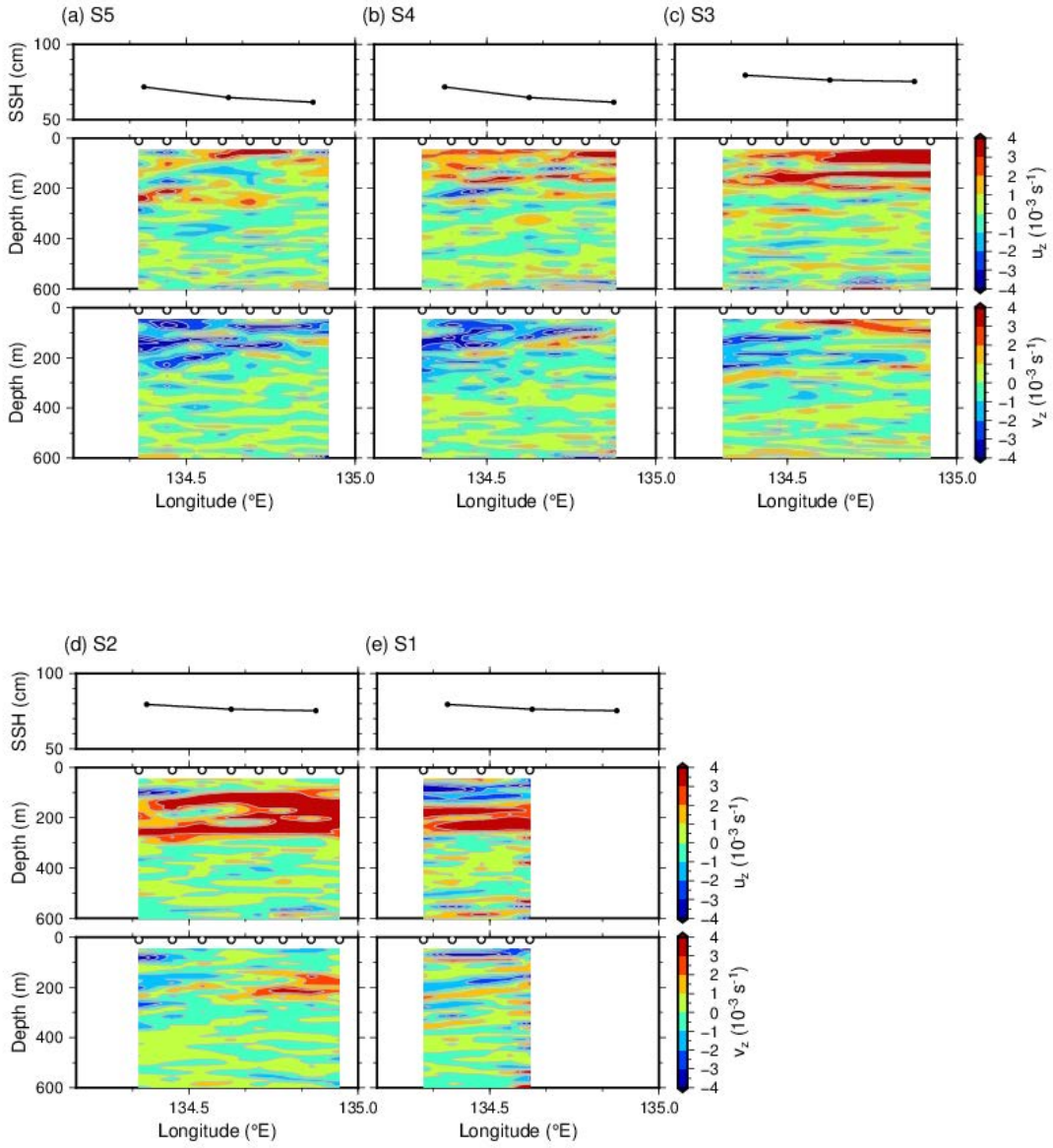

Figure 13. As in Fig. 7, but for **a**–**e** S5–S1.

3.3. XCTD

(1) Personnel

Yusuke Kawaguchi, AORI, PI

Daiki Ito, FRA

Akie Sakai, RIAM (author)

(2) Objectives

Hydrographic measurements with eXpendable Conductivity, Temperature and Depth profiler (XCTD) were performed during KS-21-12 to capture the hydrographic structure of mesoscale eddies over L-3 line.

(3) Instruments and method

The XCTD observations were carried out in the Yamato Basin along the meridional L3-line (135°12’E) from the northernmost St. L3-1 (38°36’N) to the southernmost L3-9 (37°16’N), every 10 minutes in latitude (Figure 1a). The probe type was XCTD-1N which measures temperature and conductivity of seawater underway of moving ship. Measured depth range was from the surface to approximately 1100 m. Total of 9 XCTD probes were deployed on June 27 (UTC)

(4) Time and positions from the field note

St. Name	Date	Start time	Lat (deg)	Lat (min)	Lon (deg)	Lon (min)
L3-1	2021/6/27	15:06	38	35.9794	135	11.9932
L3-2	2021/6/27	16:09	38	25.9834	135	12.0079
L3-3	2021/6/27	17:10	38	15.9934	135	12.0123
L3-4	2021/6/27	18:11	38	5.9876	135	12.0000
L3-5	2021/6/27	19:12	37	55.9831	135	12.0026
L3-6	2021/6/27	20:15	37	45.9329	135	12.0009
L3-7	2021/6/27	21:15	37	35.9827	135	11.9998
L3-8	2021/6/27	22:15	37	25.9408	135	11.9964
L3-9	2021/6/27	23:13	37	15.9747	135	12.0019

(5) Preliminary Results

Vertical cross-sections of potential temperature, salinity, and geostrophic velocities showed the structure of mesoscale eddy (Figure 2). The center of the cold eddy was around St. L3-7, since the isopycnales (> 26.4) were convex upward. The estimated

geostrophic current showed eastward and western current between Sts. L3-1 and -2, and Sts. L3-4 and -9 respectively. A high temperature and high salinity water mass was shown around the surface layer of St. L3-3, which would have been flowed from western area because of the strong eastward current (> 0.6 m s^{-1}) at the southern edge of the anticyclonic eddy (Figure 2, a, b, from St. L3-7 to the north).

Vertical profiles of temperature and salinity showed details of the water property distributions along the L3-line (Figure 1). The high salinity (> 34.4) water mass was found in the upper 100 m at St. L3-7 (Figure 1, c, red line). A step like structure was found in the range from 50 to 300 m at St. L3-8 and -9, suggesting that the bottom of

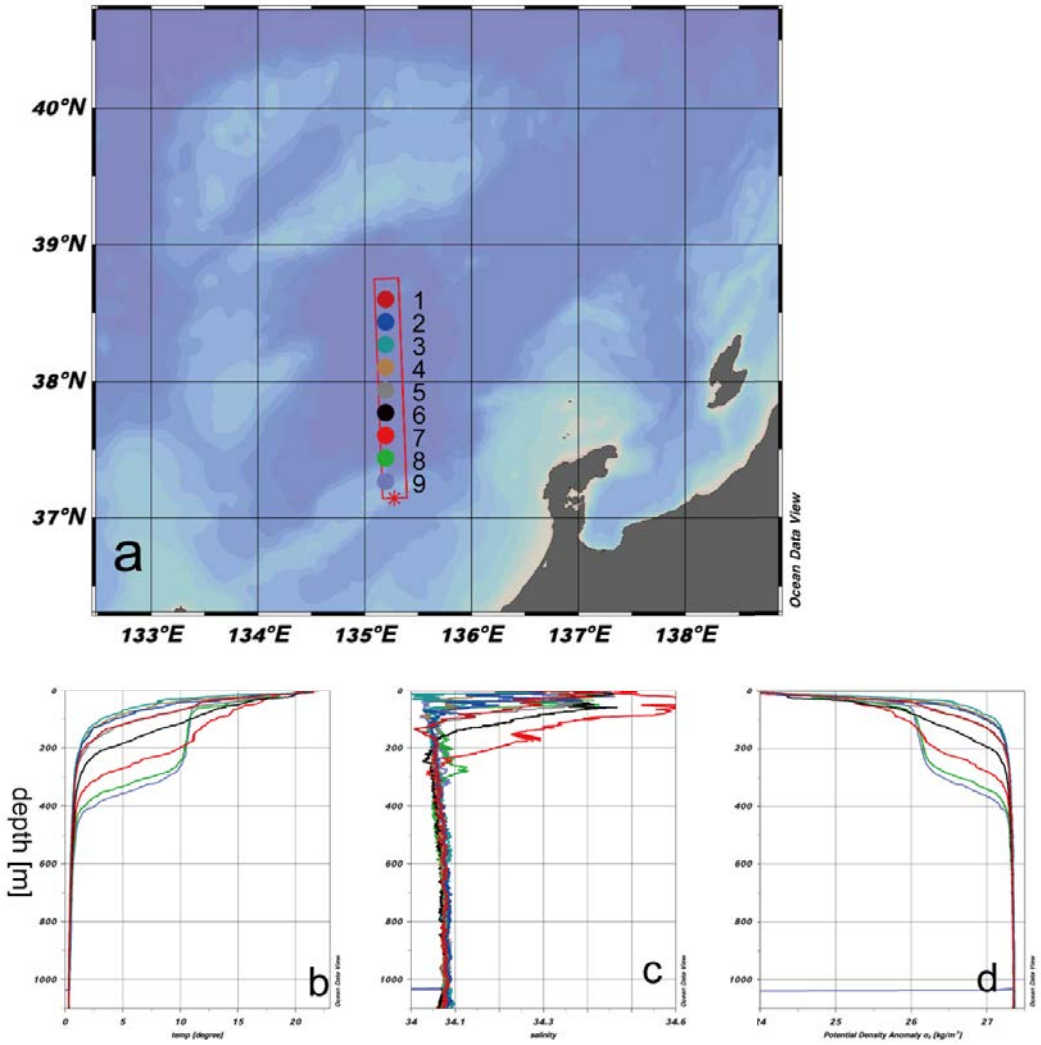

Figure 1 Preliminary results of the XCTD survey. (a) Map showing the L3-line, (b) vertical profiles of temperature, (c) salinity, and (d) potential density. The color of lines represents the color of dots in the map.

the warm eddy (from St. L3-8 to the south) was around 300 m. The Japan Sea Proper Water was found in the deeper than 500 m, since the density profiles showed uniform value at all the stations (Figure 1, d).

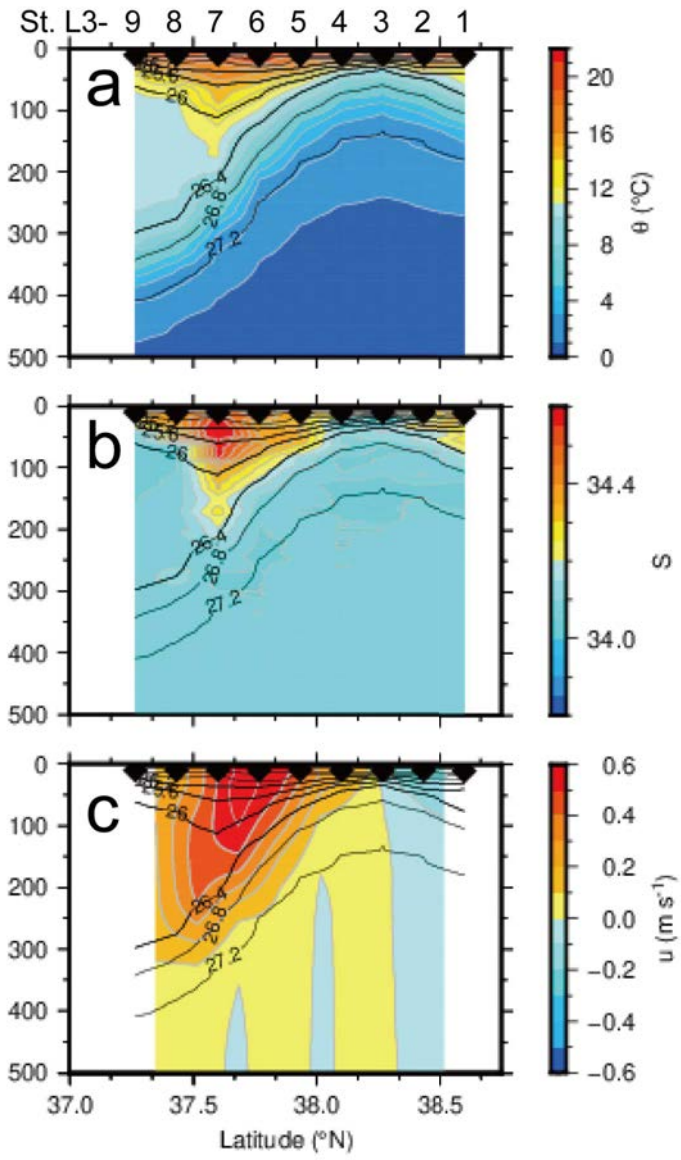

Figure 2 Preliminary results of the XCTD survey. (a) Vertical cross-sections of potential temperature, (b) salinity, (c) geostrophic velocity along line-L3 (1000 m is the layer of no motion). The black lines show the potential density.

3.4. CTD

(1) Personnel

Itsuka Yabe: AORI, principal investigator (author)

Yusuke Kawaguchi, Shinzou Fujio, Eun Yae Son, Yu Zeshu, Ahmed Sk. Istiaque: AORI

Sato Hironori: MWJ

Taku Wagawa, Daiki Ito: FRA

Tomoharu Senjyu, Akie Sakai: RIAM

(2) Objectives

CTD measurement aim to capture hydrographic structure in the Yamato Basin.

(3) Instruments and methodology

At Stn. JS-2 of the mooring position, CTD measurement was conducted from the surface nearly to the seafloor. Water samples were taken at the depths of 10, 30, 50, 100, 150, and 200 m to the purpose of the Ocean DNA.

(4) CTD deployment positions

Stn.	Date	Time (JST)	Lat (deg)	Lat (min)	Lon (deg)	Lon (min)
JS-2	20210627	0750	38	0.263	135	2.821

(5) Preliminary Results

Figure 1 indicates vertical profiles of potential temperature, salinity, potential density, and the Brunt väisälä frequency. Seasonal pycnocline was strong in the surface layer (Fig. 1c), the maximum value of the Brunt väisälä frequency was approximately 16 cph at the depth of 30 m (Fig. 1d). Warm and saline Tsushima Warm Current Water (TWCW) was observed upper 40 m (Fig. 2). Seawater properties were almost uniform deeper than 300 m where the Japan Sea Proper Water (JSPW, < 1°C) was detected (Fig. 2).

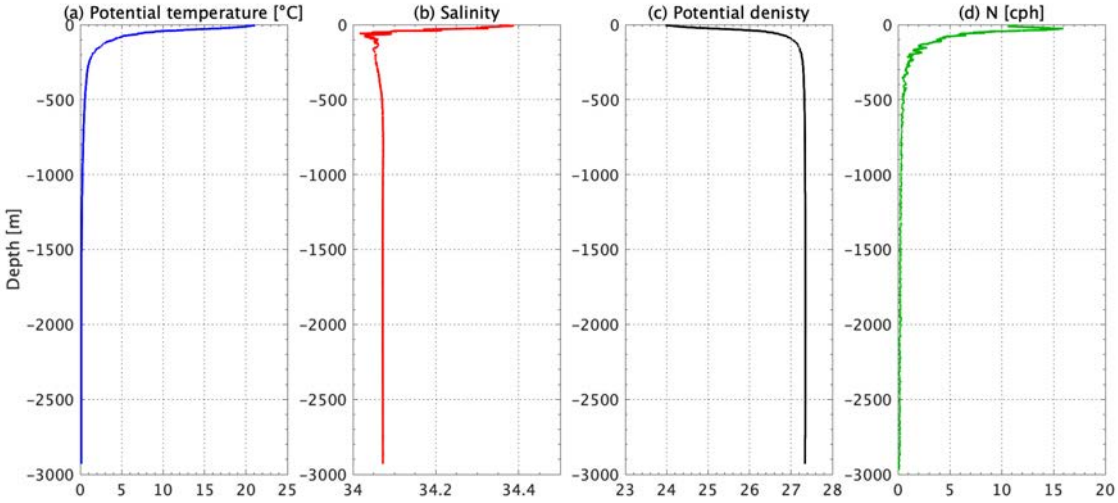

Figure 1: Vertical profile of (a) potential temperature, (b) salinity, (c) potential density, (d) Brunt-Väisälä frequency N at JS-2.

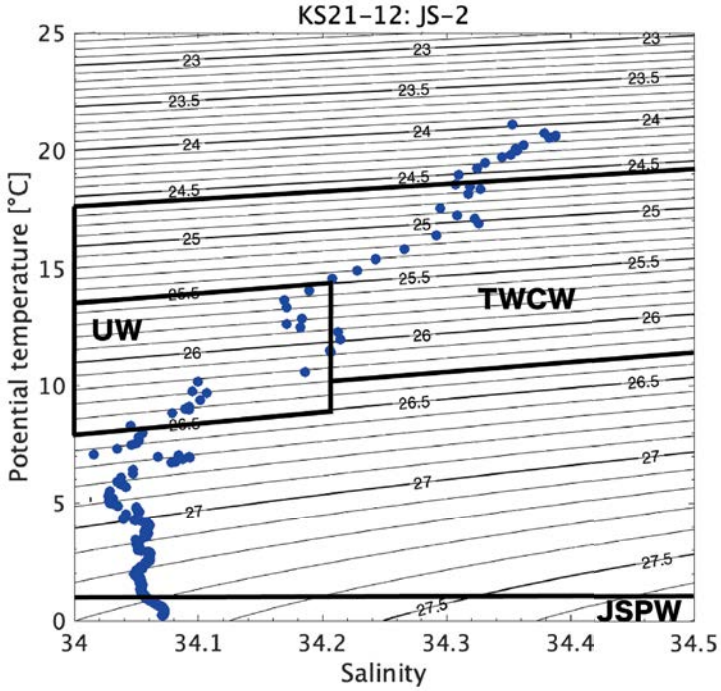

Figure 2: TS-diagram at Stn. JS-2. The contour intervals are 0.2 for thin lines, and 1.0 for thick lines. Abbreviations for water mass names are following: Upper-layer Water (UW), Tsushima Warm Current Water (TWCW), and Japan Sea Proper Water (JSPW).

3.5. LADCP

(1) Personnel

Yusuke Kawaguchi, AORI, U. Tokyo (PI)

Eun Yae Son, AORI, U. Tokyo (author)

Sato Hironori, MWJ

(2) Objectives and methodology

The lowered ADCP (LADCP), Workhorse Monitor WHM300 (Teledyne RD Instrument, San Diego, California, USA) was utilized to get a vertical profile of shear data. LADCP system consists of downward looking ADCP and a 45V battery package. The LADCP system was set for recording before the CTD cast and its data was recovered right after the cast. Velocity conversion was done by LDEO LADCP software (version 10; Visbeck 2002).

Detailed configuration is below:
Bin size: 8.0 m
Number of bins: 25
Pings per ensemble: 1
Ping interval: 1.0 sec

(3) Station log

The LADCP was utilized on June 27 at 38-00.25 °N, 135-02.79 °E.

(4) Data quality

The data conversion has been conducted using LEDO software. The beam performance from the four beams showed high percentage over 95% with the good correlation among the transducers (Figure 1). Tilt maintained near 0° and the heading kept maintained 140° during down-cast. The bottom tracking performance was okay without any errors. The shear profile from the LADCP can be seen in Figure 2.

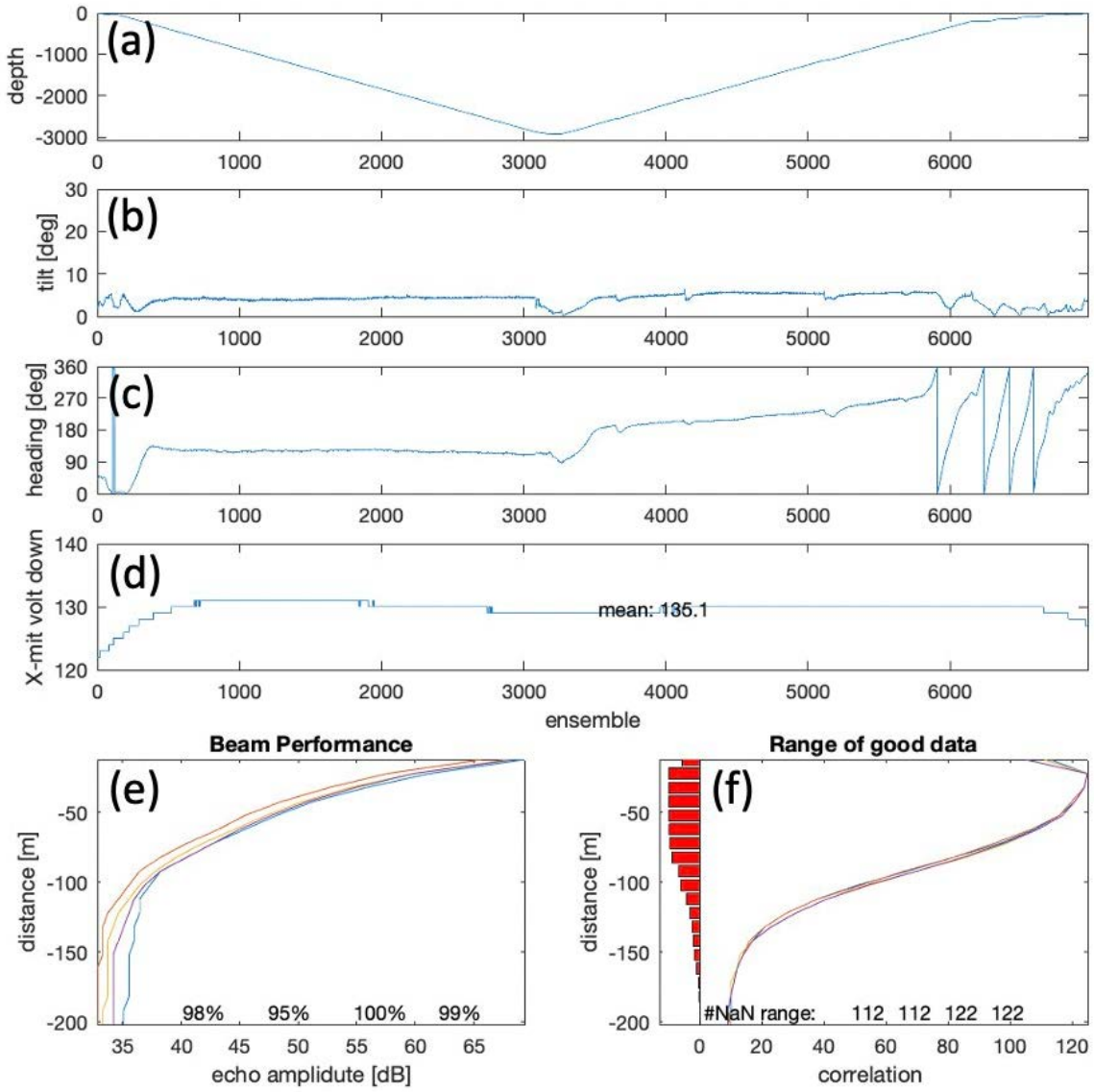

Figure 3. Information about data quality of LADCP. (a) pressure, (b) tilt, (c) heading, (d) voltage, (e) beam performance, and (f) correlation.

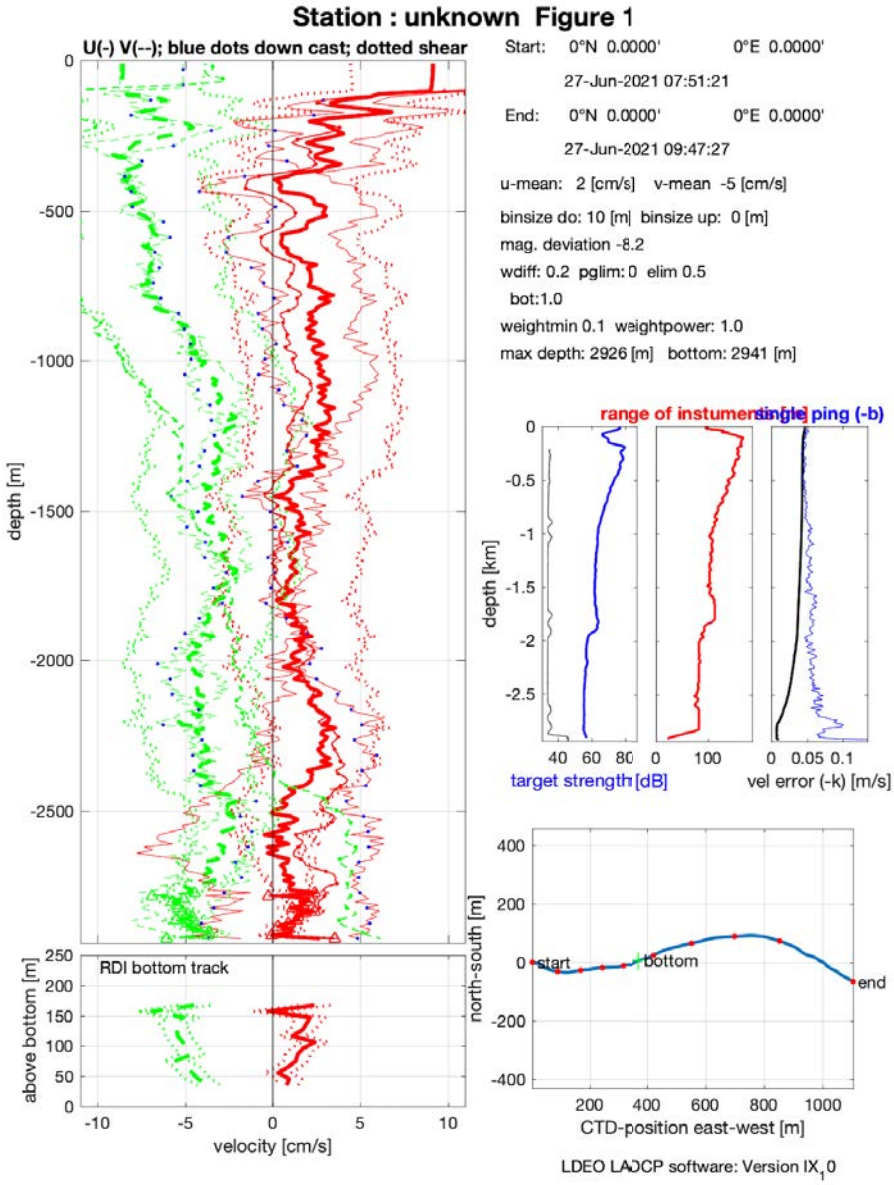

Figure 4. Example profile of converted shear data.

Reference

Visbeck, M. (2002): Deep velocity profiling using Acoustic Doppler Current Profilers: Bottom track and inverse solutions, J. Atmos. Oceanic Technol., 19, 794–807.

3.6. Mooring Observations

(1) Personnel

Yusuke Kawaguchi: AORI, principal investigator (author)
Shigeyoshi Otosaka, Shinzou Fujio, Itsuka Yabe: AORI

(2) Objectives

To acquire timeseries of temperature, salinity, and oceanic current, along with vertical transport of sediment and sinking matters, at various depths of water column in the Yamato Basin, the Sea of Japan.

(3) Instruments and methodology

The mooring was underway at the station JS-2 in nearly center of the Yamato Basin. Physical oceanographic instruments consist of three sets of current meters (including an ADCP) and two sets of CTD sensors. To get sinking particles for chemical analysis, two sets of sediment trap were installed on the mooring system. The detailed configurations are shown in a table below.

Devices	Deployed depths (target)	Sampling intervals
Teledyne WH Longranger	600 m	60 sec
Nortek AquaDopp D	1200 m	60 sec
Seabird SBE37-SM (MicroCAT)	1200 m	60 sec
Sediment trap (SMD6000W)	1200 m	5 days × 2 periods
Nortek AquaDopp D	2400 m	60 sec
Sediment trap (SMD6000W)	2400 m	5 days × 2 periods
Seabird SBE37-SM (MicroCAT)	2400 m	60 sec

(4) Deployment positions

A set of mooring system was deployed on June 27, 2020 during the KS-21-12 (current cruise) and recovered on July 11, 2020 during the KS-21-13 (directed by S. Otosaka). The accurate deployment position was re-evaluated with three times of ranging procedure onboard in several hours after the deployment.

Station	Depth(m)	Lat (deg)	Lat (min)	Lon (deg)	Lon (min)
JS-2	2973	38	0.12440	135	2.0636

(5) Preliminary Results

Every instruments on the mooring system worked properly and fully collected the 60-sec interval timeseries data, as planned. With respect to long-term average of horizontal current, it was u = 0.2 ± 11 cm s^{-1} and v = -6.6 ± 8.7 cm s^{-1} in eastward and northward velocities as an average over vertical range of 200–600 m, based on ADCP measurement (Fig. 1). From the AquaDopp current meters, deployed at mean depths of 1218 and 2430 m, the average velocities were respectively u = 2.3 ± 2.7 cm s^{-1} and v = -4.0 ± 2.5 cm s^{-1}, and u = 2.0 ± 3.5 cm s^{-1} and v = -3.7 ± 3.1 cm s^{-1} (Fig. 2). The mean current also shows some dynamic shifting around September 4, 2020, particularly manifest from the single point current meters at the different two depths. Another noticeable feature in the current is a short-term oscillation. This is likely attributable to some fluctuations in water motion due to wind-driven inertial current or similar frequency of internal waves.

With respect to the digital records from SBE37-SMs, the quality of variables taken,

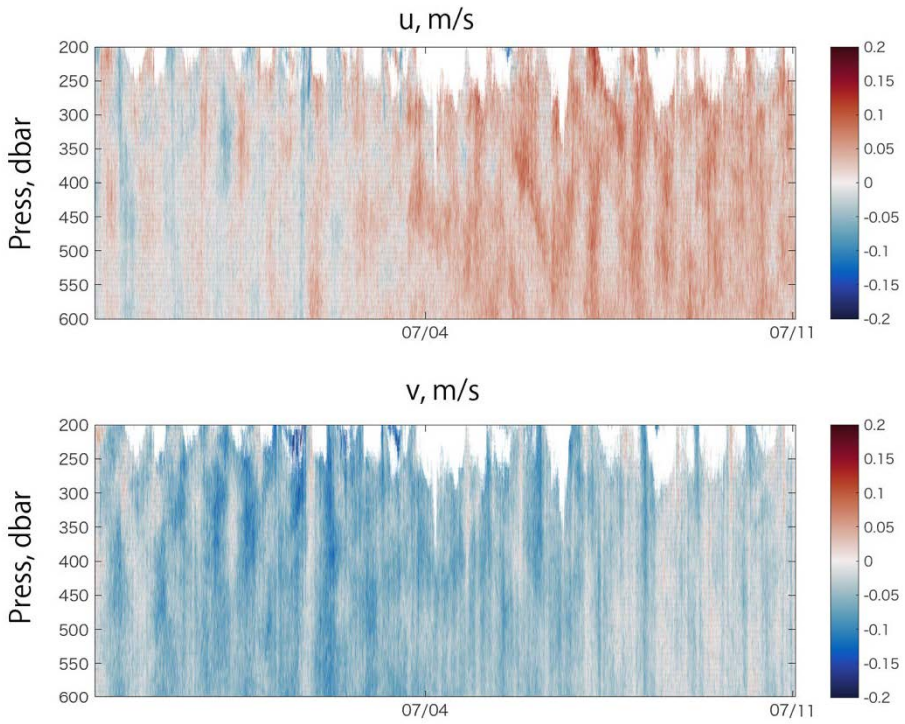

Figure 1: Time-vertical section of horizontal current from Longranger ADCP: (top) zonal and (bottom) meridional components.

including temperature, salinity and pressure, were all fine (Fig. 3). The record of nearly constant pressure (1196 ± 0.23 dbar) from the upper SBE sensor tells us that the vertical system was rarely dragged down by strong current (top panels in Fig. 3). On other hand, the deeper one shows some significant drifting by nearly +2 dbar for 2 weeks, which should be calibrated during a time of post-processing. On average, temperature and salinity at 1196 dbar are 0.2682 ± 0.0089°C and 34.069 ± 0.00041, while they at 2415 dbar are 0.26086 ± 0.00022°C and 34.066 ± 0.0008 (middle and bottom in Fig. 3). The upper-deployed CTD device records the similar variabilities that was seen in horizontal current (Fig. 2). It is characterized by the near inertial short-term fluctuation as well as a temporal depression as relatively long-term trend that occurred at center of July 4.

In the deployment of the mooring system at Station JS-2, sinking particles were successfully collected for two periods each with a sediment trap installed in two layers.
The sample was dried on a pre-weighed membrane filter having a pore size of 0.6 μm. The total mass flux calculated from the mass of the dried sample is summarized in table below.

Sampling depth (m)	Sampling date		Total mass flux (mg m^{-2} day^{-1})
	Start	End	
1219	June 29, 2021	July 3, 2021	71.6
	July 4, 2021	July 8, 2021	77.2
2431	June 29, 2021	July 3, 2021	133.0
	July 4, 2021	July 8, 2021	101.3

Comparing the mass fluxes observed in 2021 with the results conducted from 2000 to 2001 at the same station and at the same depths, no significant change was observed in the lower trap (2431 m), whereas it was about 30% lower in the upper trap (1219m). The considerable physical factors that can affect such a decrease in mass fluxes in the upper layers should be discussed in the future.
In addition, from the analysis of the elemental composition and isotopes of the sinking particles, we will discuss the sedimentation characteristics of particulate matter and changes in the transport flux of anthropogenic substances to the deep sea in the last 20 years.

Figure 2: Timeseries of horizontal current from AquaDopp current meters at average depths of 1218 m (top) and 2430 m (bottom). Please refer to color codes for current direction.

a)

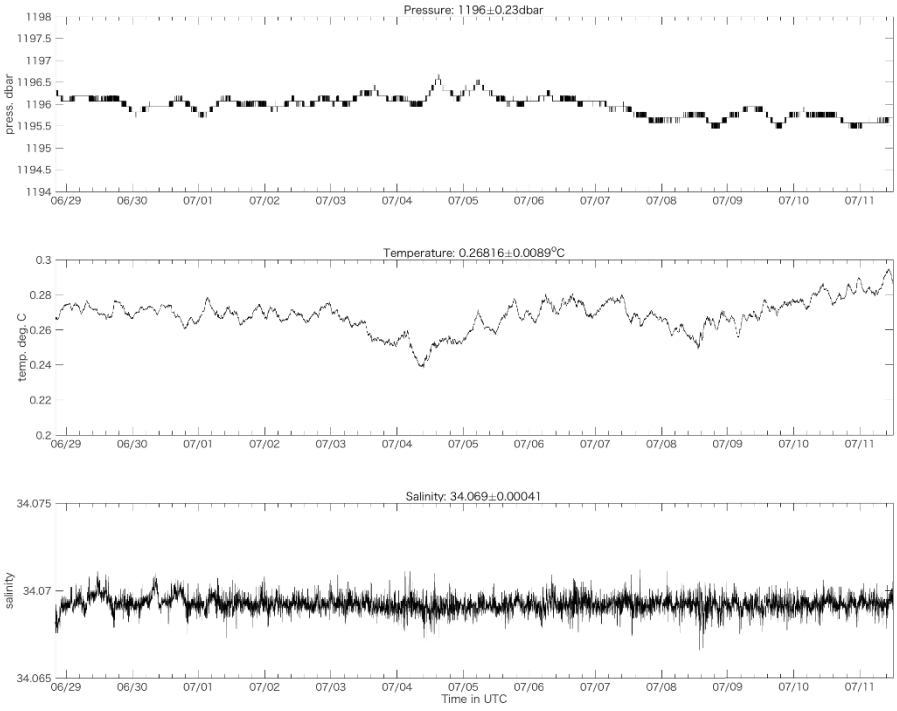

b)

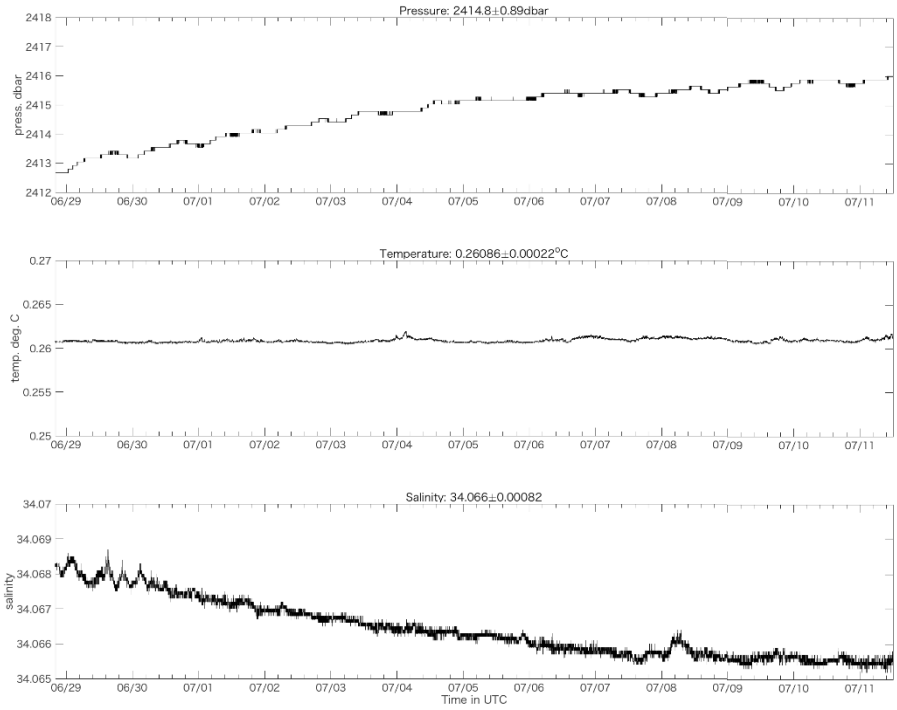

Figure 3: Timeseries of (top) pressure, (middle) temperature and (bottom) salinity from SBE37-SM at average pressures of (a) 1196 dbar and (b) 2418 dbar.

3.7. Ocean DNA

(1) Personnel

Shin-ichi, Ito (not onboard): AORI, U. Tokyo, Principal Investigator (author)
Yu Zeshu, AORI
Sk Istiaque Ahmed: AORI

(2) Objectives

OceanDNA (environmental DNA from open ocean) sampling here aims to estimate the spatial distribution structures of marine fish in the surface water of Tsushima Warm Current along with to understand and compare between the surface water samples (0m, collected by bucket) and the intake water samples from the ship bottom (here after intake samples).

(3) Instruments and methodology

In station JS-2, water samples were taken a) by the CTD-Niskin water sampling system from 10m to 200m depth; b) from the intake (came from pump in the ship bottom); c) through the bucket from ocean surface.

Along L1 & L2-lines, water samples were taken from intake and bucket in each station. On S1~S5-lines, water samples were taken from intake and bucket in every two stations. Each water sample was stored in a sterilized plastic bag and then immediately filtered using a 0.45-μm Sterivex filter unit. Each sample (in the bag) was weighed before and after the filtering. The residual water in the Sterivex filter unit was pushed out by a clean syringe. Then 2.0 mL RNAlater Stabilization Solution was added into each Sterivex filter unit. Then Sterivex filter units were all stored at -30°C until DNA extraction.

(4) Water sampling positions

A total of 86 samples were collected from 40 different stations. The positions of the water sampling stations are enlisted in the following table:

ID	Station	Depth (m)	Tube ID	60 Progress (degree-minute)		Time of Filtering (JST)	
				Latitude	Longitude	Start	End
1	JS-2	0	7A	38-00.263	135-02.821	6/27 19:35	6/27 22:00
2	JS-2	T	7B				
3	JS-2	10	7C				

4	JS-2	30	7D						
5	JS-2	50	6B					6/27	21:53
6	JS-2	100	6C					6/27	21:34
7	JS-2	150	6A					6/27	21:35
8	JS-2	200	6D					6/27	21:34
9	L2-9	0	7A	37-16.002	134-41.952	6/28	11:18	6/28	14:41
10	L2-9	T	7B					6/28	14:35
11	L2-8	0	7D	37-26.5083	134-42.0431	6/28	13:00	6/28	15:55
12	L2-8	T	7C					6/28	15:55
13	L2-7	0	6B	37-36.0389	134-42.1003	6/28	14:28	6/28	17:45
14	L2-7	T	6D					6/28	17:45
15	L2-6	0	6A	37-45.9814	134-42.0242	6/28	16:01	6/28	19:19
16	L2-6	T	6C					6/28	18:30
17	L2-5	0	7D	37-55.9695	134-41.9593	6/28	17:35	6/28	21:00
18	L2-5	T	7A					6/28	21:01
19	L2-4	0	7B	38-05.933	134-41.919	6/28	19:10	6/28	21:14
20	L2-4	T	7C					6/28	21:16
21	L2-3	0	6B	38-15.975	134-41.960	6/28	20:42	6/28	23:25
22	L2-3	T	6C					6/28	23:33
23	L2-2	0	6A	38-25.973	134-41.955	6/28	22:32	6/29	01:45
24	L2-2	T	6D					6/29	01:45
25	L2-1	0	7C	38-36.008	134-41.921	6/29	00:15	6/29	03:03
26	L2-1	T	7A					6/29	03:03
27	L1-1	0	7B	38-35.9492	134-12.0128	6/29	02:55	6/29	05:52
28	L1-1	T	7D					6/29	05:52
29	L1-2	0	6D	38-25.9465	134-11.9843	6/29	04:22	6/29	07:43
30	L1-2	T	6A					6/29	07:45

31	L1-3	0	6B	38-	134-	6/29	05:50	6/29	07:46
32	L1-3	T	6C	06.9474	11.9507			6/29	08:43
33	L1-4	0	7A	36-	134-	6/29	07:08	6/29	09:55
34	L1-4	T	7B	05.9559	12.0177			6/29	09:55
35	L1-5	0	7C	37-	134-	6/29	08:35	6/29	10:46
36	L1-5	T	7D	55.2619	11.8540			6/29	10:46
37	L1-6	0	6B	37-	134-	6/29	09:55	6/29	13:13
38	L1-6	T	6C	45.962	12.179			6/29	14:46
39	L1-7	0	6A	37-	134-	6/29	11:44	6/29	14:59
40	L1-7	T	6D	35.936	11.988			6/29	14:49
41	L1-8	0	7A	37-	134-	6/29	13:25	6/29	16:56
42	L1-8	T	7B	26.0784	12.0122			6/29	16:56
43	L1-9	0	7C	37-	134-	6/29	14:44	6/29	18:01
44	L1-9	T	7D	15.9948	11.9635			6/29	18:01
45	S3-9	0	6D	37-	134-	6/29	17:40	6/29	19:25
46	S3-9	T	6A	41.172	17.000			6/29	19:47
47	S3-7	0	6C	37-	134-	6/29	21:06	6/29	23:40
48	S3-7	T	6B	41.179	26.984			6/29	22:40
49	S3-5	0	7A	37-	134-	6/29	23:14	6/30	01:38
50	S3-5	T	7B	41.178	37.052			6/30	01:12
51	S3-3	0	7C	37-	134-	6/30	01:10	6/30	03:26
52	S3-3	T	7D	41.2173	47.0504			6/30	03:26
53	S3-1	0	6D	37-	134-	6/30	02:49	6/30	05:34
54	S3-1	T	6A	41.2291	37.1156			6/30	05:34
55	S2-2	0	6B	37-	134-	6/30	05:23	6/30	08:08
56	S2-2	T	6C	36.1926	52.1194			6/30	08:06
57	S2-4	0	7A	37-	134-	6/30	07:40	6/30	10:09
58	S2-4	T	7B	36.154	42.141			6/30	10:05
59	S2-6	0	7C	37-	134-	6/30	10:15	6/30	12:30
60	S2-6	T	7D	36.166	32.053			6/30	12:25
61	S2-8	0	6A	37-	134-	6/30	12:20	6/30	15:23
62	S2-8	T	6D	36.2057	21.9831			6/30	14:50
63	S4-9	0	6B	37-	134-	6/30	15:10	6/30	17:34
64	S4-9	T	6C	48.0059	17.0164			6/30	17:36
65	S4-7	0	7A	37-	134-	6/30	17:10	6/30	19:28

66	S4-7	T	7B	47.9287	26.9652			6/30	19:15
67	S4-5	0	6A	37-	134-	6/30	19:40	6/30	21:32
68	S4-5	T	6D	47.928	32.098			6/30	21:30
69	S4-3	0	6C	37-	134-	6/30	21:18	7/01	01:54
70	S4-3	T	6B	48.005	47.092			6/30	23:22
71	S4-1	0	6D	37-	134-	6/30	23:15	7/01	01:55
72	S4-1	T	6A	48.016	57.055			7/01	01:55
73	S5-2	0	7B	37-	134-	7/01	1:53	7/01	04:05
74	S5-2	T	7A	59.9418	52.0122			7/01	04:00
75	S5-4	0	7C	37-	134-	7/01	3:50	7/01	06:30
76	S5-4	T	7D	59.9392	41.9999			7/01	06:20
77	S5-6	0	6A	37-	134-	7/01	5:42	7/01	08:15
78	S5-6	T	6D	59.9620	31.9885			7/01	08:06
79	S5-8	0	6B	37-	134-	7/01	7:33	7/01	09:45
80	S5-8	T	6C	59.954	21.932			7/01	09:52
81	S1-9	0	7C	37-	134-	7/01	11:42	7/01	15:11
82	S1-9	T	7D	33.223	16.953			7/01	14:02
83	S1-7	0	7B	37-	134-	7/01	13:29	7/01	16:27
84	S1-7	T	7A	31.1952	26.9968			7/01	16:18
85	S1-5	0	6B	37-	134-	7/01	15:18	7/01	18:02
86	S1-5	T	6C	31.2453	37.0425			7/01	18:02

*T: intake water sample

(5) Preliminary Results

The DNA extraction for all the collected samples have been finished for further analysis (metabarcoding with MiFish and quantitative PCR (q-PCR) analysis for small pelagic fish). It will require some more time to finish the final analysis, but it is expected to finish within the end of 2021. After obtaining the result, we will process data according to our research objectives. Main topics are 1) compare OceanDNA results between intake and bucket samples to test the validity of OceanDNA analysis using intake water, 2) compare fish community structure detected by metabarcoding with the ocean water mass structure, 3) compare small pelagic fish distribution detected by qPCR with the ocean water mass structure.

3.8. pCO_2 Observation

(1) Personnel

Takafumi Aramaki (not onboard): NIES, Principal Investigator

Tomoharu Senjyu, RIAM (author)

(2) Objectives & Methods

To observe the oceanic net CO_2 flux in the Japan Sea, we installed a suite of partial pressure of CO_2 (pCO_2) analytical equipment on board (Photo 1). The surface water for research drawn into the ship was used for the pCO_2 measurements. The pCO_2 was observed at intervals of 1 second from the departure of Kochi Port to the arrival at Maizuru Port. In addition, temperature and salinity of the surface water that was taken from the same tap of the pCO_2 sampling were measured with a T-S meter manufactured by JFE Advantech (ACTW-USB) at intervals of 10 seconds (Photo 2).

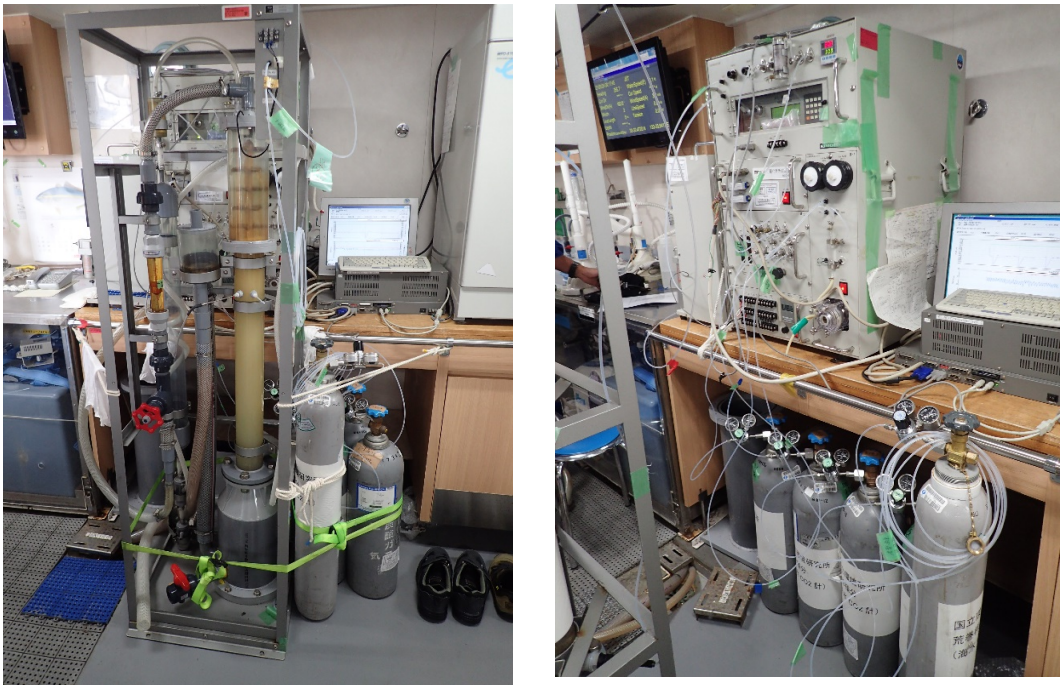

Photo 1: pCO_2 observation equipment installed in the laboratory

Photo 2 The T-S meter for the measurements of temperature and salinity of the surface water which was taken from the same tap of the pCO_2 sampling

4. Final remarks and future perspectives

The present science cruise, KS-21-12, was planned as the second field program of survey in the framework of an inter-organizational collaboration project, the FRA-AORI Tsushima Warm Current Observatory (FATO). The first FATO cruise was implemented in October, 2019 with the same vessel of R/V Shinsei-maru, identified as KS-19-21, in which the research region was by the TWC front, farther northeast off the Sado Island (Kawaguchi et al. 2021). Differently from the previous cruise, KS-21-12 was targeted at more stably existing WCR that is known to frequently appear in the Yamato Basin. The mesoscale features related to the TWC is temporally quite dynamic. This therefore makes very hard to prospect the exact locations of TWC axis and WCR for the observational stations. The use of forecasting model output was new attempt, which could lead reduced failures in pre-determination of observational positions and allow us flexible changes for the activities even in middle of the cruise. Combining the satellite-based sea-surface height (or absolute dynamics topography) and the MRI forecast would provide further advantages in terms of geographical accuracy accessing the targets.

The output from the three-dimensional MRI model would be prospecting so it enables the detailed inspection of meso- and submeso-structures that the shipboard survey focused on in the real ocean. The microscale turbulent mixing may be parameterized by giving some a priori constants in the model. The field-based correction for turbulent mixing would improve the quality by suggesting optimal functions or coefficients that empirically explain the real ocean’s physical phenomena. Arrays of vertical slices of shipboard ADCP observation could definitely illustrate clues and help increased understanding about the fine-scale filaments that go around meso-structures of TWC front and WCR. In the future analyses with the data acquired, close inspections of straining of velocity field will be progressed. This hopefully elucidates the essences of inter-scale energy transfer related to energy cascading from (to) smaller-scale turbulence to (from) larger-scale front dynamics via the submeso-scale.

References:

Kawaguchi, Y., Wagawa, T., Yabe, I., Ito, D., Senjyu, T., Igeta, Y., Ito, S., (2021). Mesoscale dependent near-inertial internal waves and microscale turbulence in the Tsushima Warm Current, J. Oceanography, doi:10.1007/s10872-020-00583-1.

5. Notice on Using

This cruise report is a preliminary documentation as of the end of cruise.
This report is not necessarily corrected even if there is any inaccurate description (i.e. taxonomic classifications). This report is subject to be revised without notice. Some data on this report may be raw or unprocessed. If you are going to use or refer the data on this report, it is recommended to ask the Chief Scientist for latest status.
Users of information on this report are requested to submit Publication Report to Cooperative Research Cruise office.

E-mail: kyodoriyo@aori.u-tokyo.ac.jp

新青丸研究航海報告

航海番号：　KS-21-12 次研究航海

航海名称：　日本海対馬暖流域における学際的合同海洋観測 I：海洋渦に捕捉される風成内部波の痕跡とその可視化
Interdisciplinary research program across the regions of Tsushima Warm Current — Part I: 3D visualization of wind-generated fine-scale internal waves associated with oceanic eddies

観測海域：　日本海、大和海盆
Yamato Basin, Sea of Japan

航海期間：　令和 3 年 6 月 25 日（金）～令和 3 年 7 月 2 日（金）

出航日時・場所　6 月 25 日 12:00 高知港

入港日時・場所　7 月 2 日 10:00 舞鶴港

主席研究員：　川口　悠介・東京大学大気海洋研究所・助教

研究内容：

1. メソ・サブメソ渦と内部波エネルギーの立体的構造・分布に関する調査
   川口　悠介：乱流・CTD・船底 ADCP
2. 大和暖水渦での沈降物資のフラックス観測
   乙坂　重嘉：係留系・セジメントトラップ・ADCP・CTD
3. 表層のメソ海洋構造に対する Ocean DNA に関する調査
   伊藤　進一：バケツ採水・DNA 分析

乗船研究者

氏名	所属	職位
川口　悠介（主席）	東大大気海洋研	助教
和川　拓（次席）	水研機構	研究員
藤尾　伸三（次々席）	東大大気海洋研	准教授
伊藤　大樹	水研機構	研究員
千手　智晴	九州大学応力研	准教授
矢部　いつか	東大大気海洋研	大学院生
孫恩愛	東大大気海洋研	大学院生
酒井　秋絵	九州大学応力研	大学院生
Yu Zeshu	東大大気海洋研	大学院生
Sk. Istiaque Ahmed	東大大気海洋研	大学院生

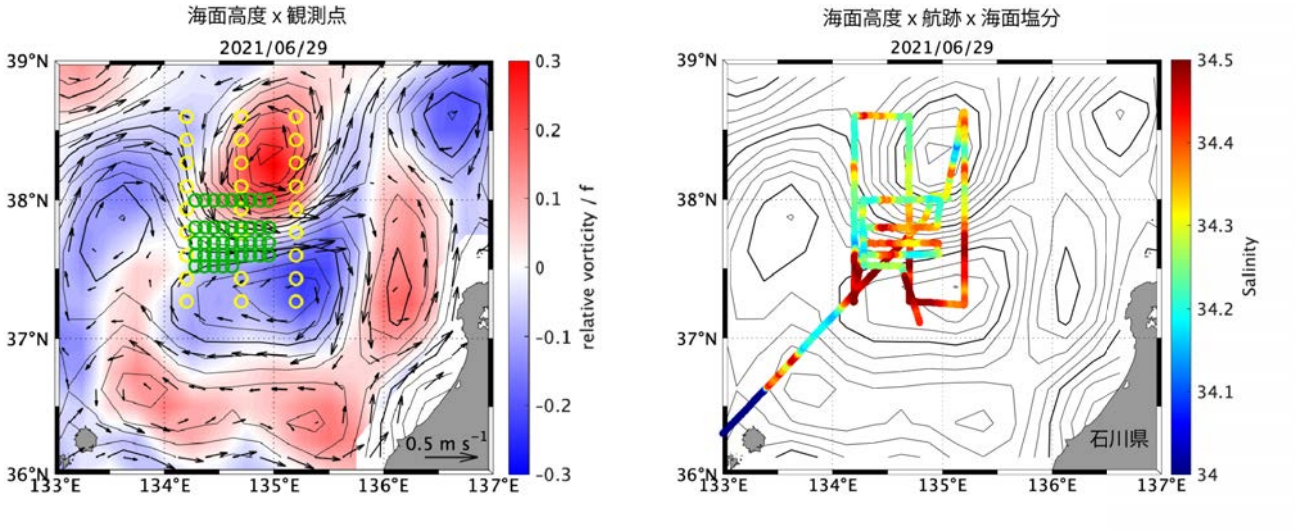

図：主な観測点（左）と航跡（右）。

左：6 月 29 日時点での海面高度を色で、地衡流をベクトルで表示。

右：海面高度を等値線で、航跡沿いの海面塩分を色で表示。